

## Evaluation of urban heat islands using local climate zones and the influence of sea-land breeze

Xilin Zhou<sup>a,\*</sup>, Tsubasa Okaze<sup>b</sup>, Chao Ren<sup>c</sup>, Meng Cai<sup>d</sup>, Yasuyuki Ishida<sup>a</sup>, Hironori Watanabe<sup>e</sup>, Akashi Mochida<sup>a</sup>

<sup>a</sup> Department of Architecture and Building Science, Graduate School of Engineering, Tohoku University, Japan

<sup>b</sup> School of Environment and Society, Tokyo Institute of Technology, Japan

<sup>c</sup> The Faculty of Architecture, The University of Hong Kong, Hong Kong

<sup>d</sup> School of Architecture, The Chinese University of Hong Kong, Hong Kong

<sup>e</sup> Department of Architecture, Faculty of Engineering, Tohoku Institute of Technology, Japan



### ARTICLE INFO

#### Keywords:

Local climate zone  
Geographic information system (GIS)  
Urban heat island (UHI)  
Land surface temperature (LST)  
Air temperature  
Sea-land breeze

### ABSTRACT

The Local Climate Zone (LCZ) scheme is an urban form and land cover/land use classification system used to study urban heat islands (UHIs). Many studies have evaluated the relationship between LCZs and air temperature. While the intensity and spatial pattern of an UHI can be influenced by the land-sea breeze, especially in coastal cities, few studies have been done to examine this using the LCZ scheme. In this study, Sendai, Japan, has been selected as a case study to evaluate whether the LCZ scheme can be used to study UHIs that are exposed to sea-land breeze since it has two urban-rural areas: mountain side and coastal side. UHI analysis was based on LCZ classes with GIS-derived geometric and land cover properties. By dividing Sendai into two regions along its urban center, the mitigating effects of sea-land breeze on the magnitudes of UHIs in each urban-rural area were demonstrated. Based on the results of this study, two specific UHI mitigation strategies were proposed for Sendai. This study confirmed that the LCZ scheme can be used by urban planners to assess both surface UHI (SUHI) and UHI effects, and proposed a feasible process for developing targeted UHI mitigation strategies.

### 1. Introduction

Rapid urbanization has caused a series of environmental problems in recent decades and this trend is continuing, especially in developing regions such as Asian and sub-Saharan African countries (Jones, 2017; Parnell & Walawage, 2011). Given climate change and high population density, cities in developing countries are vulnerable; however, their urban morphological data and land cover information may not be standardized, available, or accessible for environmental research and future local development. The Local Climate Zone (LCZ) scheme is a climate-related classification of homogenous urban structures and land cover types introduced by Stewart and Oke (2012), that has been adopted world-wide as an international standard for climate-related studies (Alexander, Bechtel, Chow, Fealy, & Mills, 2016; Brousse, Martilli, Foley, Mills, & Bechtel, 2016; Giridharan & Emmanuel, 2018; Kaloustian & Bechtel, 2016; Kotharkar & Bagade, 2018). The LCZ scheme was originally designed for observational urban heat island (UHI) studies and includes 17 standard types–10 classes for built types

and 7 classes for land cover types—that can be divided into sub-classifications, according to local needs and situations (Bechtel et al., 2015; Stewart & Oke, 2012). Recently, LCZ data has been used for other urban climate studies, including energy, air pollution distribution patterns, and thermal comfort (Lau, Chung, & Ren, 2019; Shi, Lau, Ren, & Ng, 2018; Tse et al., 2018).

Studies of methods for delineating LCZ classifications can generally be divided into two categories: GIS-based methods and satellite-based methods (Gál, Bechtel, & Unger, 2015; Kotharkar & Bagade, 2018; Wang, Middel et al., 2018; Wang, Ren, Xu, Lau, & Shi, 2018). The GIS-based methods delineate LCZ types using calculated building parameters and vegetation indicators; the building data can be obtained from commercial data, Open Street Maps (OSMs), or government databases that calculate morphology parameters, and the vegetation data can be obtained from the Normalized Difference Vegetation Index (NDVI) or Land Use Land Cover (LULC) databases, which include parameters for land cover types (Geletič & Lehnert, 2016; Lelovics, Unger, Gál, & Gál, 2014; Zheng et al., 2018). The satellite-based

\* Corresponding author at: Dept. of Architecture & Building Science, Graduate School of Engineering, Tohoku University, Aoba 6-6-11-1205, Sendai, 980-8579, Miyagi, Japan.

E-mail address: [zhouxilin@sabine.pln.archi.tohoku.ac.jp](mailto:zhouxilin@sabine.pln.archi.tohoku.ac.jp) (X. Zhou).

**Table 1**

Satellite images acquired for LCZ classification and LST analysis.

Satellite image	Entity ID	Date	Satellite image	Entity ID	Date
Landsat 8	LC08_L1TP_107033_20150502_	05/02/2015	Landsat 7	LE07_L1TP_107033_20151017	10/17/2015
	LC08_L1TP_107033_20150806	08/06/2015			
	LC08_L1TP_107033_20151212	12/12/2015	Aster	SC: AST_08.003:2179595158	07/29/2015
	LC08_L1TP_107033_20160317	03/17/2016		SC: AST_08.003:2127457027	09/18/2013

methods employ supervised learning to evaluate satellite images and choose training samples (Bechtel & Daneke, 2012; Xu, Ren, Cai, Edward, & Wu, 2017). These are the prevailing methods for delineating LCZ classifications according to the World Urban Data Access Portal Tool (WUDAPT), as they are an easy-to-operate method based on free software and input data (Bechtel et al., 2015).

Stewart, Oke, and Krayenhoff (2014) verified that the LCZ scheme can use the inter-zone temperature difference at screen height ( $\Delta T_{LCZ\ X-Y}$ ) to quantify heat island magnitude, and other studies have reported accurate performance of the LCZ scheme based on air temperature data from fixed-station observations, mobile measurements, and numerical simulations (Stewart et al., 2014; Alexander & Mills, 2014; Fenner, Meier, Scherer, & Polze, 2014; Leconte, Bouyer, Claverie, & Pétrissans, 2015; Thapa Chhetri, Fujimori, & Moriaki, 2017; Beck et al., 2018; Shi et al., 2018; Verdonck et al., 2018). While the land surface temperature (LST), which can be used to represent the surface urban heat island (SUHI), has been shown to be generally consistent with LCZ classifications (Geletić, Lehnhert, & Dobrovolný, 2016; Wang, Middel et al., 2018; Wang, Ren et al., 2018; Cai, Ren, Xu, Lau, & Wang, 2018; Yang et al., 2019), few studies have considered the influence of sea-land breeze on UHIs when evaluating LCZs, as the majority of conventional study areas are located in plains or basins that do not have significant differences in elevation.

Sendai, Japan is a mountain-coastal city with horizontal expansion and an elevation difference of 200 m in urban areas. There are two types of urban-rural areas in Sendai – the mountain side with high elevation and the coastal side with low elevation – and unlike some mountain-coastal cities such as Hong Kong, the urban areas in Sendai are not close to the coastline. Sasaki, Mochida, Yoshino, Watanabe, and Yoshida (2008) studied heat-island effects using the regional characteristics of heat-balance mechanisms in Japanese cities and demonstrated that during the day, lower elevation areas are exposed to the cooling effects of sea breeze more than higher elevation areas. This result implies that sea breeze may affect UHI intensity during the day, and nighttime wind from the mountain side may also contribute to the differences in UHI intensity between high and low elevation areas.

The main objective of this study is to evaluate whether the LCZ scheme can serve as a tool for UHI studies in Sendai, which is exposed to sea-land breeze. To that end, this study has three sub-objectives: 1) evaluate the accuracy of LCZ maps developed with the WUDAPT Level 0 (L0) method, using a confusion matrix and derived geometric and surface cover properties from GIS methods; 2) illustrate SUHI profiles by calculating the mean LST for each LCZ type as a reference for UHI studies; and 3) demonstrate how sea-land breeze affects the magnitude of two different UHIs in Sendai, one in each of the two urban-rural areas, by analyzing the air temperature differences between LCZs using data obtained from fixed stations.

## 2. Study area

The megacities in Japan include Tokyo's 23 Special Wards and the system of designated cities (Ohsugi, 2011). As of the middle of 2019, there were 20 designated cities, and these cities were home to 21.65 %

of the total population of Japan in 2015. Sendai occupies an area of 786 km<sup>2</sup> and had a population of 1.08 million in 2015 (Population census of Japan, 2015); therefore, Sendai is ranked in the middle of the system of designated cities, which suggests it is a typical designated city in Japan.

Sendai is located in northeastern Japan along the pacific coast and it has a humid subtropical climate, classified as Cfa by the Köppen climate classification system (Peel, Finlayson, & McMahon, 2017). As the nearest major city to the 2011 Tohoku earthquake and tsunami, Sendai suffered huge losses (Hiraishi, Yoneyama, Baba, & Azuma, 2014); however, Sendai has still experienced relatively high population growth, as its growth rate was 3.46 % from 2010 to 2015, which is close to the 3.66 % growth rate of the Tokyo Special Wards (Population census of Japan, 2015).

## 3. Materials and methods

### 3.1. LCZ classification using the WUDAPT method

The WUDAPT L0 method is designed for universal use, with free data and software available. Delineating LCZ classifications using the WUDAPT L0 method has three main steps: 1) preprocessing Landsat images obtained from the USGS Earth Explorer; 2) creating and selecting LCZ training samples in Google Earth; and 3) conducting LCZ classification using the Random Forest algorithm in Saga GIS. Steps 2) and 3) are iterative processes, to get satisfactory results (Bechtel et al., 2015).

In this study, we selected four groups of multi-spectral images from Landsat 8 Operational Land Imager (OLI)/Thermal Infrared Sensors (TIRS) Level-1, representing four seasons in Sendai from 05/02/2015 to 03/17/2016, with the criteria of availability and cloud coverage of less than 10 % (Table 1). All the bands in each group were then clipped by the region of interest (ROI) and resampled from 30 m to 100 m resolution using the nearest neighbor method. Fifteen types of LCZs were identified in Sendai, according to the LCZ scheme obtained using the 3D view in Apple Maps 3D. However, LCZ 2<sub>4</sub> (compact middle-rise with open high-rise) and LCZ 4<sub>2</sub> (open high-rise with compact middle-rise) areas were not large enough to be treated as unique climate areas; thus, they were classified as LCZ 2 (compact middle-rise) and treated as 'homogenous' urban structures. Similarly, LCZ 3<sub>5</sub> (compact low-rise with open mid-rise) was classified as LCZ 3 (Fig. 1). Therefore, training samples for 13 LCZ types, including 7 built types and 6 land-cover types, were selected in Google Earth. Five to twenty training polygons for each LCZ type were selected, based on WUDAPT criteria for training areas greater than 1 km<sup>2</sup>.

The training areas (TAs) and Landsat multi-spectral images were used as the Saga GIS input data for a random forest algorithm. Because LCZ specifies that homogenous urban structures and land-cover types greater 1 km<sup>2</sup> are needed (Bechtel et al., 2015), a 3 × 3 pixels majority filter was used to erase fragments during post-processing. In order to assess the classification accuracy, a set of independent validation samples was randomly selected, based on the digital land use map of Sendai (Urban Development Bureau of Sendai, 2016), to compare with



**Fig. 1.** Training examples for LCZ mapping in Sendai, Japan, obtained using Apple Maps 3D.

the LCZ map classifications, using a confusion matrix. The details of Landsat 7 Enhanced Thematic Mapper Plus (ETM+) products for total shortwave albedo (ALB) calculation and Advanced Spaceborne Thermal Emission and Reflection Radiometer (ASTER) products adopted for LST analysis (Table 1) are discussed in Section 3.2.5 and 3.3.1, respectively.

### 3.2. Deriving geometric, surface cover and radiative properties of LCZ built types

Stewart and Oke (2012) defined the standard 17 types of LCZs with specific ranges of geometric and surface cover, thermal, radiative, and metabolic properties. In order to assess the properties of LCZ built types in Sendai, building height (BH), building surface fraction (BSF), sky view factor (SVF), pervious surface fraction (PSF), and total shortwave albedo (ALB) parameters (all included in the definition of LCZs) were selected. Both BH and BSF are the key parameters for classifying LCZ built types. The former can be used to classify the high-rise, middle-rise, low-rise built types, and the latter can be adopted to classify the compact, open, sparsely building types. While SVF and PSF are well-known parameters for urban climate research, the radiative property of ALB, which is the key variable for radiation energy budget of the land surface, was selected for LST analysis.

These parameters were generated within each grid cell of the LCZ map at 100 m resolution and compared with those suggested by Stewart and Oke (2012). The BH, BSF, and SVF were calculated using the building polygons in the 2018 GIS data of the Tohoku region of Japan. Since buildings such as large commercial centers and public transportation stations can exceed the area of a grid cell (Ng, Yuan, Chen, Ren, & Fung, 2011), the shapefiles of large buildings were clipped by the fishnet of the LCZ map to avoid cross-region building polygons.

#### 3.2.1. Building height

Building height represents the average building height in each grid cell of the LCZ map (Salamanca, Martilli, Tewari, & Chen, 2011; Xu, Ren, Ma et al., 2017; Zheng et al., 2018):

$$BH = \frac{\sum_{i=1}^n (BH_i * BA_i)}{\sum_{i=1}^n BA_i} \quad (1)$$

where  $BA_i$  is the footprint area of a building,  $BH_i$  is the building height, and  $n$  is the total number of buildings in a grid cell.

#### 3.2.2. Building surface fraction

The BSF is the percentage of a building's footprint relative to the grid cell's area:

$$BSF = \frac{\sum_{i=1}^n BA_i}{A_{grid}} \quad (2)$$

where  $BA_i$  is the footprint area of a building,  $A_{grid}$  is the area of one grid cell ( $100 \times 100$  m), and  $n$  is the total number of buildings in a grid cell.

#### 3.2.3. Pervious surface fraction

The PSF can be estimated by assuming that the surface of an urban area only includes vegetation cover and impervious surfaces (Kaspersen, Fensholt, & Drews, 2015; Van de Voorde, Jacquet, & Canters, 2011). In this study, the Landsat 8 L1 product of Sendai on a summer day (08/06/2015) was used to calculate PSF as fractional vegetation cover with the Normalized Difference Vegetation Index (NDVI) proposed by Carlson and Traci Arthur (2000):

$$NDVI = \frac{\rho_{NIR} - \rho_R}{\rho_{NIR} + \rho_R} \quad (3)$$

$$\text{PSF} = \left( \frac{\text{NDVI} - \text{NDVI}_0}{\text{NDVI}_s - \text{NDVI}_0} \right)^2 \quad (4)$$

where  $\rho_{NIR}$  and  $\rho_R$  are the top of atmosphere (TOA) reflectance acquired in the red (band 4) and near-infrared (band 5) regions, respectively (Weir & Herring, 2000), and  $\text{NDVI}_0$  and  $\text{NDVI}_s$  are the value of soil NDVI (non-vegetated surface) and highest value of NDVI (dense vegetation) in the area of interest, respectively.

### 3.2.4. Sky view factor

The SVF was calculated using the SVF tool in SAGA GIS (Conrad et al., 2015), which is based on building vector data and a digital elevation model (DEM) raster file (Fig. 3b). The vector file of building polygons from the Sendai GIS data was transferred to a raster file with 2 m resolution and masked on the corresponding DEM raster file, which was resampled from 5 m to 2 m resolution. The masked raster file was used as the input data for SAGA GIS. While the high resolution digital surface model (DSM) method for directly calculating SVF may seem to be more effective (Zheng et al., 2018), the DEM-based method tends to be more cost-effective in Japan, as 30 m resolution DSM images are freely available to the public, whereas 5 m resolution DEM images can be downloaded from the Geospatial Information Authority of Japan (GSI) for free. Furthermore, only values for the ground were extracted from the 2 m resolution SVF map, with values for the tops of buildings excluded. The SVF, with 100 m resolution for calculating average SVF of each LCZ built type, was generated in each LCZ grid cell using the following equation:

$$\text{SVF} = \frac{\sum_{i=1}^n \text{SVF}_i}{n} \quad (5)$$

where  $\text{SVF}_i$  is the SVF value of a pixel from the ground-extracted SVF map with 2 m resolution, and  $n$  is the total number of pixels in one grid cell of the LCZ map.

### 3.2.5. Total shortwave albedo

The ALB is a kind of land surface broadband albedo. Liang (2001) proposed a number of simple formulae to estimate average ALB from various narrowband sensors. Among those sensors, the Landsat 7 ETM + had shown the second-best performance, only slightly lower than the Moderate Resolution Imaging Spectroradiometer (MODIS). While the resolution of shortwave bands from the MODIS instrument is 250–500 m, the 30 m resolution shortwave bands from Landsat 7 ETM + on a clear day (Table 1) were adopted to be resampled into 100 m resolution by the nearest neighbor method for matching the resolution of the LCZ map. The mean ALB was estimated by the following equation:

$$\text{ALB} = 0.356\alpha_1 + 0.13\alpha_2 + 0.373\alpha_4 + 0.085\alpha_5 + 0.072\alpha_7 - 0.0018 \quad (6)$$

where the  $\alpha_i$  is the TOA reflectance available in band  $i$  from Landsat 7 ETM + instrument.

### 3.3. Evaluating temperature variation of LCZs

Air temperature data obtained from nearby meteorological observation stations was used to evaluate the thermal differences between LCZs. This method has been widely used to verify LCZs (Alexander & Mills, 2014; Thapa Chhetri et al., 2017); however, site locations and natural wind may substantially affect the accuracy of UHI analysis. Therefore, LST data derived from satellite images was used as a reference for the SUHI analysis, because it can provide continuous surface temperature data, which can be used to prevent analytical differences due to location and temporal factors. Both LST and air temperature data were used to evaluate thermal differentiation between LCZs in Sendai.

### 3.3.1. Land surface temperature

The surface kinetic temperature product (AST\_08) of ASTER is widely used for LST data (Cai et al., 2018; Middel, Brazel, Kaplan, & Myint, 2012; Myint, Wentz, Brazel, & Quattrochi, 2013; Wang, Middel et al., 2018; Wang, Ren et al., 2018). The AST\_08 includes surface temperature data with 90 m spatial resolution over land areas, and is based on Planck's Law and emissivity values from the Temperature-Emissivity Separation (TES) algorithm (NASA LP DAAC, 2001). Free, daily LST products such as MODIS Land Surface Temperature and Emissivity (MOD11) is only up to 1 km resolution (Wan, 2013), which is much coarser than the resolution of LST data from AST\_08; however, using LST products from Landsat 8 data will affect the independence of the resultant LCZs (Li & Jiang, 2018) and only the daytime images of Landsat 8 are available free. Therefore, AST\_08 products were the optimal choice for this study. Two AST\_08 images—acquired during the night (10:30 pm) on July 29th (Fig. 2a) and during the day (10:30 am) on September 26th (Fig. 2b)—were used for the hot, summer LST analysis (Table 1). The images were chosen based on availability and cloud cover (less than 10 %).

### 3.3.2. Air temperature measurements

The local prevailing wind direction in summer is from the southeast (Junimura & Watanabe, 2008). To assess the influence of mountain-sea breeze on UHIs, thirteen of twenty-two fixed loggers were selected and separated into two groups, named Line P and Line Q, based on the diurnal (9:00–18:00, JST) and nocturnal (21:00–5:00, JST) prevailing wind directions obtained from the one-hour averaged wind data of the Automated Meteorological Data Acquisition System (AMeDAS). (Fig. 3 a, b) Because winds from the sea or the mountains have different magnitudes of thermal impact on areas with different elevations (Sasaki et al., 2008), the Line P and Line Q measurements can also be distinguished with different changes in elevation. The largest elevation difference in Line P was approximately 200 m, while the loggers in Line Q only differed by up to 60 m in elevation (Fig. 3b). Loggers WP, CP, and EP, which were located at the west point, center point, and east point of the study area, respectively, were part of both Line P and Line Q.

All the loggers were set 1.5 m above the ground and housed in Stevenson screens. Each instrument shelter was located in an open space with good ventilation, near or inside a primary school. (Fig. 3c, d) Air temperature measurements were acquired every 10 min during August, the hottest month in Sendai (August 1–31, 2018). In order to eliminate the uncertainty caused by consecutive rainy days, only the data obtained between August 11th and 22nd was used; during this time window, it only rained during the night of August 15th and during the day on August 16th.

## 4. Results and analysis

### 4.1. Accuracy of LCZ maps generated for Sendai, Japan

Fig. 4a shows the LCZ map of Sendai generated by the WUDAPT L0 method at 100 m resolution. As shown in Fig. 4a and Table 2, the vegetation in western and northern Sendai is composed of forest (LCZ A), while the eastern and southern areas are farmland (LCZ D); forestland occupies 34.22 % of land area and farmland occupies 18.39 %. Urban areas cover 43.89 % of the land and are divided into three regions, based on two wind corridors over rivers that run in the east-west direction. The overall urban area is dominated by LCZ 3 (compact low-rise) and LCZ 6 (compact mid-rise), which cover 11.20 % and 12.78 %, respectively. To the west of the urban areas, the land is mainly covered by large low-rise buildings (LCZ 8), which occupy approximately 10 % of the land in Sendai.

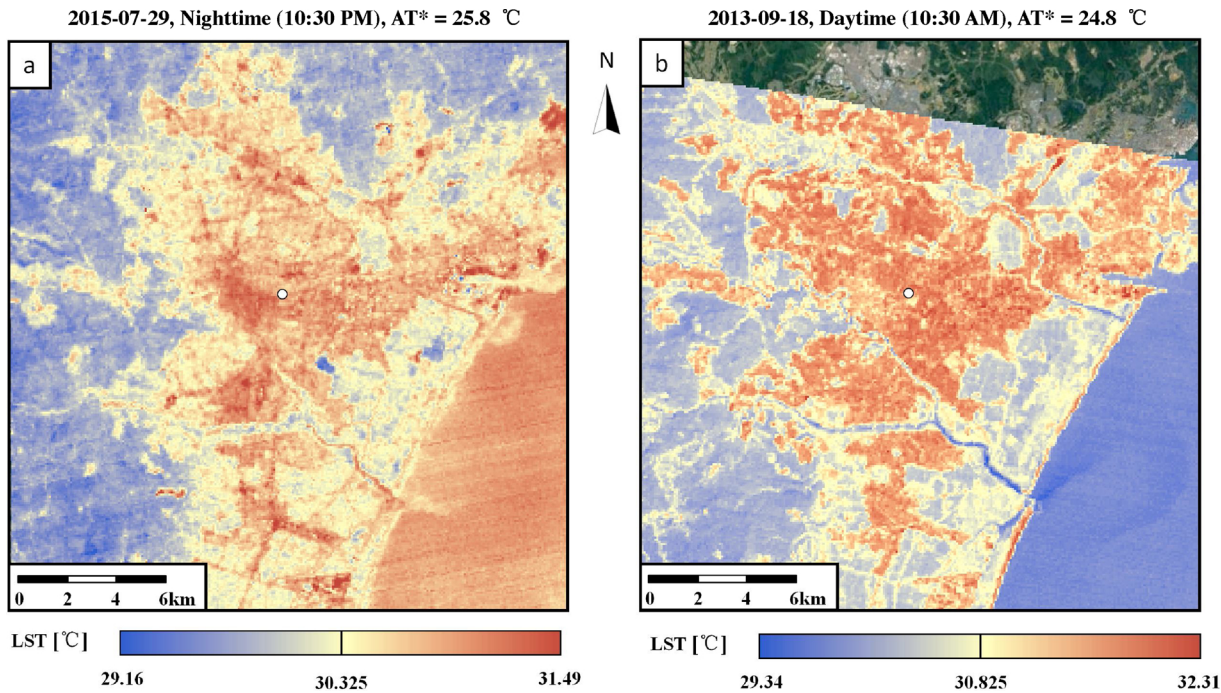


**Fig. 2.** (a) Nighttime and (b) daytime LST images of Sendai, Japan from the ASTER satellite; AT\* is the air temperature observed by the weather station located at the white circle (elevation: 38.9 m; Japan Meteorological Agency).

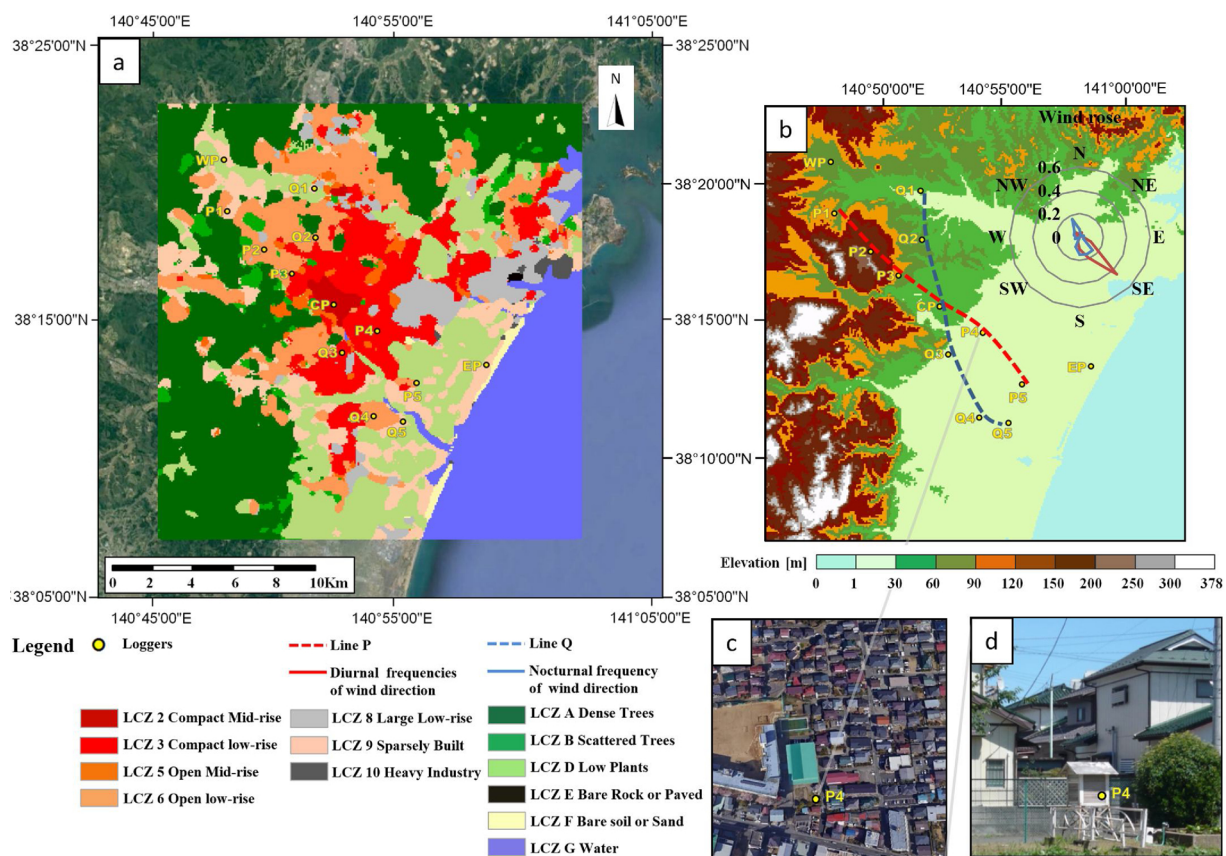


**Fig. 3.** Locations of fixed loggers measuring the air temperature on the (a) LCZ map and (b) DEM map; the location of logger P4 (c) on Google Earth and (d) in a photograph of the real site.

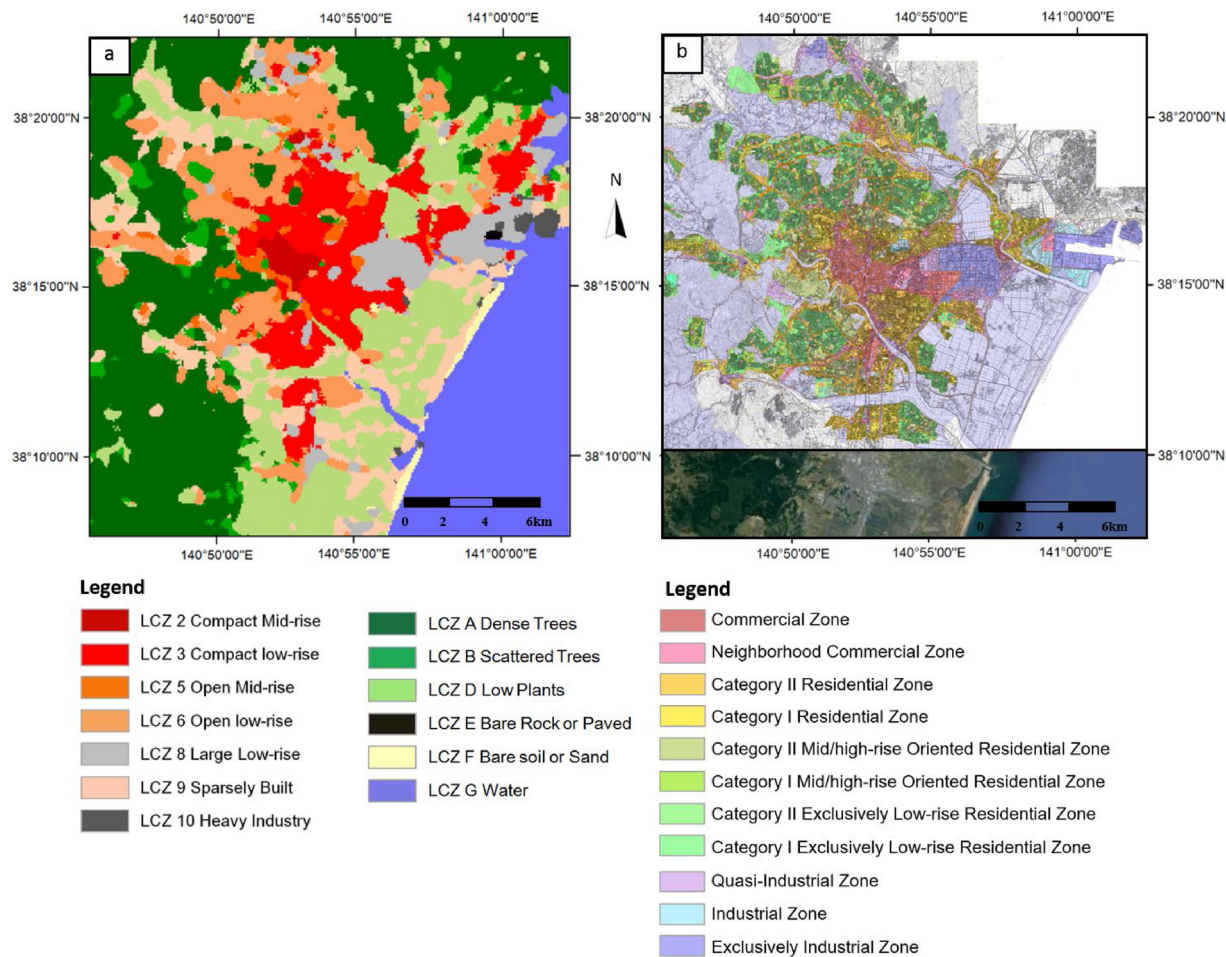


**Fig. 4.** (a) LCZ map with 100 m resolution-filtered; (b) land use map of Sendai.

Reference samples with 2768 pixels in total were selected in Google Earth for comparison. Since the land cover types were easy to recognize, only the samples of built types were selected, based on the digital land use map of Sendai (Urban Development Bureau of Sendai, 2016; Figure 4b). The number of reference pixels for each LCZ type is shown in the sum column of the confusion matrix (Table 3). The relationships of the reference samples and land use categories are listed in Table 4. Details of the characteristics of land use categories in Japan are shown in Fig. A1.

The overall accuracy and kappa coefficient of the LCZ classifications are 92.59 % and 91.71 %, respectively (Table 3), which indicates that the classification results are satisfactory. Some misclassifications were still identified in sparsely built (LCZ 9) and low plants (LCZ D) areas, as the LCZ 9 training samples included some farmland pixels; 54 of the 298 LCZ 9 pixels were misclassified as LCZ D.

**Table 2**  
Land area proportion of each LCZ.

LCZ	Area Proportion (%)	LCZ	Area Proportion (%)
LCZ 2 (compact mid-rise)	0.85	LCZ A (dense trees)	34.22
LCZ 3 (compact low-rise)	11.20	LCZ B (scattered trees)	2.77
LCZ 5 (open mid-rise)	2.20	LCZ D (low plants)	18.39
LCZ 6 (open low-rise)	12.78	LCZ E (bare rock or paved)	0.07
LCZ 8 (large low-rise)	5.86	LCZ F (bare soil or sand)	0.67
LCZ 9 (sparsely built)	10.38		
LCZ 10 (heavy industry)	0.64		

#### 4.2. Geometric and surface cover properties of LCZ built types in Sendai, Japan

##### 4.2.1. Maps of geometric, surface cover and radiative properties

Fig. 5 shows the geometric and surface cover maps of BH, BSF, PSF, and SVF as well as the radiation map derived using the ALB. These maps are consistent with the LCZ maps of Sendai.

In the BH and BSF maps of Sendai, the urban area exhibits a circular gradient with three levels that decrease away from the city center (Fig. 5a, b). Mid- and high-rise buildings that are mainly used for commercial and business affairs are clustered in the city center, which explains the maximum BH and BSF values in the inner circle of Sendai. Conversely, two-story dwellings dominate the outer ring, which has the lowest building coverage ratio, while some 3–9 story buildings are scattered among the compact two-story dwellings in the middle ring. The urban structure of Sendai is also reflected in the SVF map (Fig. 5e,

**Table 3**

Confusion matrix for LCZ classification of Sendai, Japan.

CLASS	Reference												Sum Row	User Accuracy	
	LCZ 2	LCZ 3	LCZ 5	LCZ 6	LCZ 8	LCZ 9	LCZ 10	LCZ A	LCZ B	LCZ D	LCZ E	LCZ F	LCZ G		
LCZ classification output	LCZ 2	120	0	0	0	0	0	0	0	0	0	0	0	120	1.00
	LCZ 3	1	238	6	10	14	4	0	0	1	0	0	0	274	0.87
	LCZ 5	0	2	92	7	2	3	0	0	4	0	0	0	110	0.84
	LCZ 6	1	8	1	159	0	5	0	0	4	0	0	0	178	0.89
	LCZ 8	2	7	4	4	295	4	1	0	0	0	0	0	317	0.93
	LCZ 9	0	0	3	8	0	226	0	0	12	0	6	0	255	0.89
	LCZ 10	0	0	0	0	1	0	89	0	0	0	0	0	90	0.99
	LCZ A	0	0	0	0	0	0	309	12	0	0	0	0	321	0.96
	LCZ B	0	0	0	8	0	2	0	0	249	0	0	0	259	0.96
	LCZ D	0	0	1	1	0	54	0	0	2	212	0	0	270	0.79
	LCZ E	0	0	0	0	0	0	0	0	0	23	0	0	23	1.00
	LCZ F	0	0	0	0	0	0	0	0	0	0	27	0	27	1.00
	LCZ G	0	0	0	0	0	0	0	0	0	0	0	524	524	1.00
Sum Column		124	255	107	197	312	298	90	309	284	212	23	33	524	
Output Accurate		0.97	0.93	0.86	0.81	0.95	0.76	0.99	1.00	0.88	1.00	1.00	0.82	1.00	
Overall Accuracy		0.9259													
Kappa Coefficient		0.9171													

f).

The PSF is a key factor for urban climate research and is shown in Fig. 5c. The PSF map clearly distinguishes the spatial distribution of vegetation and built types; however, the water in the PSF map was masked by the LCZ 17 layer in the LCZ map, because the PSF value of water was similar to that of the urban area. The ALB map in Fig. 5d shows the total shortwave albedo for each pixel in ROI ranges from 0 to 0.52. In the urban area, even though the ALB ranges show very small

differences from 0 to 0.17, a higher ALB in the urban center was found when it was compared to the surrounding urban areas.

#### 4.2.2. Analysis of geometric, surface cover, and radiative properties

The average geometric, surface cover, and radiative values of each LCZ built types are listed in Table 5 and the LCZ parameter ranges determined for Sendai are compared to those proposed by Stewart and Oke (2012) in Fig. 6. The maximum and minimum of each parameter

**Table 4**

Land use zone categories for standard and sub-class LCZ built types in Sendai (Japan International Cooperation Agency, 2007; Urban Development Bureau of Sendai, 2016).

LCZ Standard classes	LCZ Sub-Classes	Land Use Zone category	Max. BCR to the site area <sup>a</sup> (%)	Max. FAR to the site area <sup>a</sup> (%)	Permitted building types
LCZ 2	LCZ 2 <sub>4</sub> ; LCZ 4 <sub>2</sub>	Commercial Zone	80	400, 600, 700, 800	Banks, cinema, restaurants, department stores; residential buildings & small factory buildings
LCZ 3	LCZ 3 <sub>5</sub>	Category I Residential Zone	60	200	Residential buildings; shops, offices, and hotels with a floor area < 3000 m <sup>2</sup>
		Category II Residential Zone	60	200	Residential buildings; shops, offices, and hotels, as well as buildings with karaoke booths
		Category I Exclusively Low-rise Residential Zone	50	80	See in permitted building types of LCZ 6
LCZ 5	LCZ 5 <sub>6</sub>	Category I Mid/high-rise Oriented Residential Zone	60	200	Medium to high residential buildings; hospital and university buildings; Certain types of shop buildings with a floor area < 150 m <sup>2</sup>
		Category II Mid/high-rise Oriented Residential Zone	60	200	Medium to high residential buildings; hospital and university buildings; certain types of shop building with a floor area < 1500 m <sup>2</sup>
		Neighborhood Commercial Zone	80	300	Daily shopping facilities; Residential, shop buildings, small factory buildings
LCZ 6	LCZ 6 <sub>E</sub> <sup>b</sup>	Category I Exclusively Low-rise Residential Zone	40, 50	60, 80	Low rise residential buildings; Low rise residential buildings which are also used as small shops or offices; elementary/junior high buildings
		Category II Exclusively Low-rise Residential Zone	50	80	Low rise residential buildings; Elementary junior high school buildings; Certain types of shop buildings with a floor area < 150 m <sup>2</sup>
LCZ 8	-	Areas where no Land Use Zones are designated	-	-	-
LCZ 9	LCZ 9 <sub>E</sub>	Quasi-Industrial Zone	60	200	Light industrial facilities and service facilities
		Industry Zone	60	200	All types of factory building; Residential and shop buildings
		Exclusively Industrial Zone	60	200	All types of factory buildings
LCZ 10	LCZ 10 <sub>E</sub>	Exclusively Industrial Zone	60	200	All types of factory buildings

<sup>a</sup> Maximum values of BCR and FAR in the site area for each LUZ are diverse in different areas of various Japanese cities.

<sup>b</sup> "E" in LCZ 6<sub>E</sub> is the bare rock or paved (LCZ E) surface.

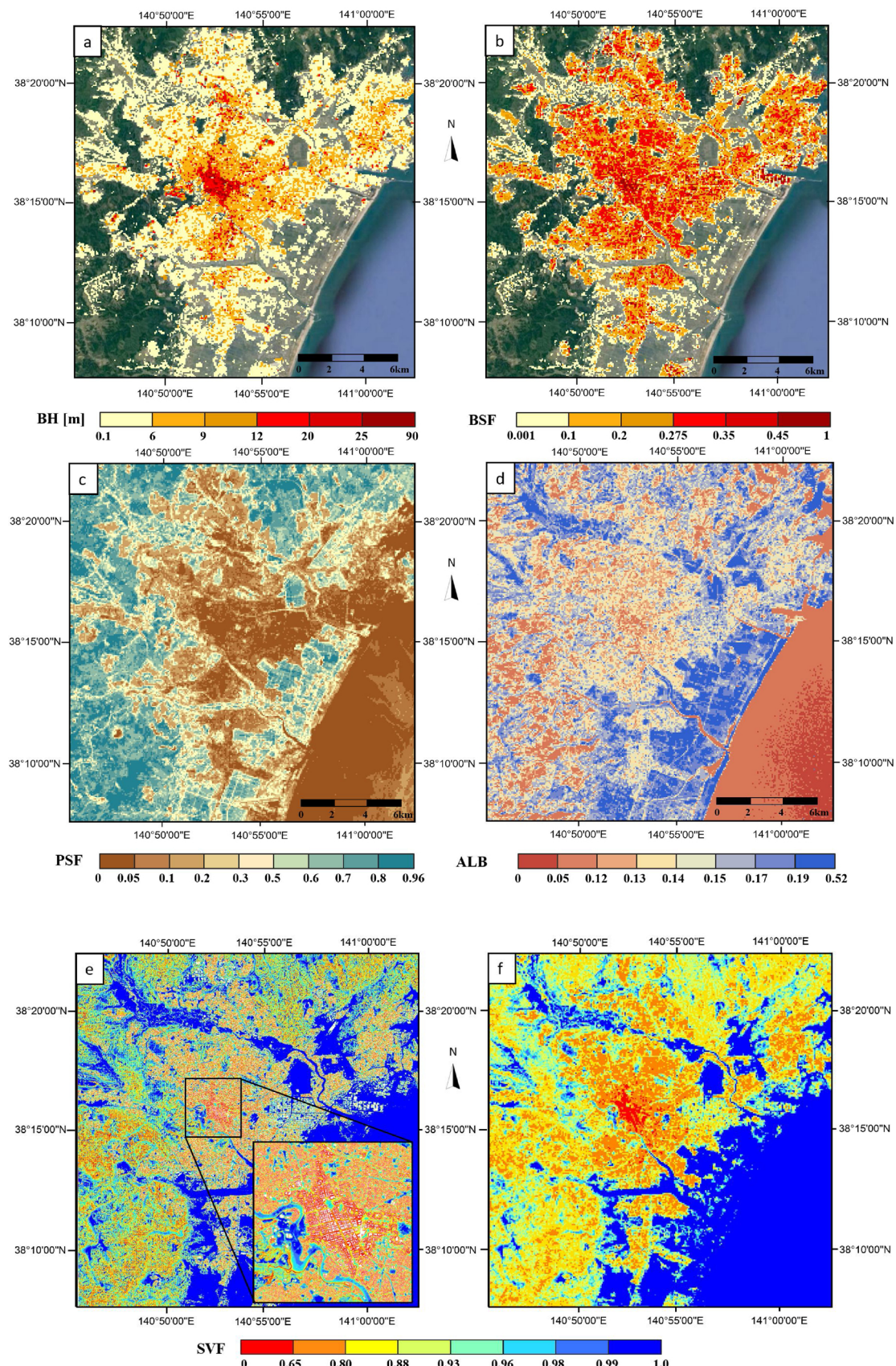


**Fig. 5.** Maps of the properties of LCZs with 100 m resolution: (a) BH, (b) BSF, (c) PSF, (d) ALB; maps of SVF with (e) 2 m resolution and (f) 100 m resolution.

**Table 5**

Geometric, surface cover, and radiative properties of the LCZ built types in Sendai and the ranges proposed by [Stewart and Oke \(2012\)](#).

LCZ	BH (m)			BSF			SVF			PSF			ALB		
	Mean	SD	Stewart & Oke	Mean	SD	Stewart & Oke	Mean	SD	Stewart & Oke	Mean	SD	Stewart & Oke	Mean	SD	Stewart & Oke
LCZ 2 (compact mid-rise)	19.61	9.98	10–25	0.29	0.13	0.4–0.7	0.67	0.14	0.3–0.6	0.04	0.04	< 0.2	0.13	0.01	0.10 – 0.20
LCZ 3 (compact low-rise)	7.21	2.41	3–10	0.26	0.08	0.4–0.7	0.79	0.07	0.2–0.6	0.08	0.04	< 0.3	0.14	0.01	0.10 – 0.20
LCZ 5 (open mid-rise)	9.15	5.15	10–25	0.14	0.11	0.2–0.4	0.88	0.08	0.5–0.8	0.17	0.11	0.2–0.4	0.15	0.02	0.12 – 0.25
LCZ 6 (open low-rise)	6.52	2.01	3–10	0.21	0.09	0.2–0.5	0.82	0.08	0.6–0.9	0.16	0.09	0.3–0.6	0.14	0.02	0.12 – 0.25
LCZ 8 (large low-rise)	7.53	3.66	3–10	0.22	0.16	0.3–0.5	0.90	0.07	> 0.7	0.05	0.04	< 0.2	0.16	0.02	0.15 – 0.25
LCZ 9 (sparsely built)	6.31	1.55	3–10	0.06	0.07	0.1–0.2	0.94	0.07	> 0.8	0.34	0.17	0.6–0.8	0.17	0.02	0.12 – 0.25
LCZ 10 (heavy industry)	7.00	2.65	5–15	0.12	0.13	0.2–0.4	0.95	0.06	0.6–0.9	0.07	0.05	0.4–0.5	0.18	0.03	0.12 – 0.20

range in Sendai were the sum and the difference between the mean and the standard deviation (SD), respectively. The coincident range represents the overlap between a property range in Sendai and that in the LCZ definition made by [Stewart and Oke \(2012\)](#).

Among these parameters, the average ALBs of each LCZ built type can be divided into the ranges proposed by [Stewart and Oke \(2012\)](#), while the average BHs can be generally matched. The average BH of LCZ 5 is slightly lower than the recommended range, due to the fact that some low-rise buildings around the open middle-rise buildings were classified as LCZ 5 in the process of selecting training samples.

Discrepancies between the average values and recommended ranges were observed in the BSFs, SVFs, and PSFs. ([Table 5](#), [Fig. 6](#)) While the

coincident ranges exist for the BSF, SVF, and PSF of some LCZ built types, the mean BSF values of all LCZs in Sendai were less than the minimum values of the recommended ranges. Furthermore, while the mean SVFs of LCZs 2, 3, 5, and 10 in Sendai were greater than the maximum values of the recommended ranges, the PSFs of LCZs 5, 6, 9, and 10 in Sendai were lower than those given by [Stewart and Oke \(2012\)](#). These discrepancies may be the result of wide streets, open parks, and parking lots being counted as LCZ built types by the mapping process, since these structures are more common in Japan.

According to the discrepancies found in [Fig. 6](#) and the observations in the process of selecting training samples, the specific sub-class LCZ built types for Sendai, are defined and listed in [Table 4](#).

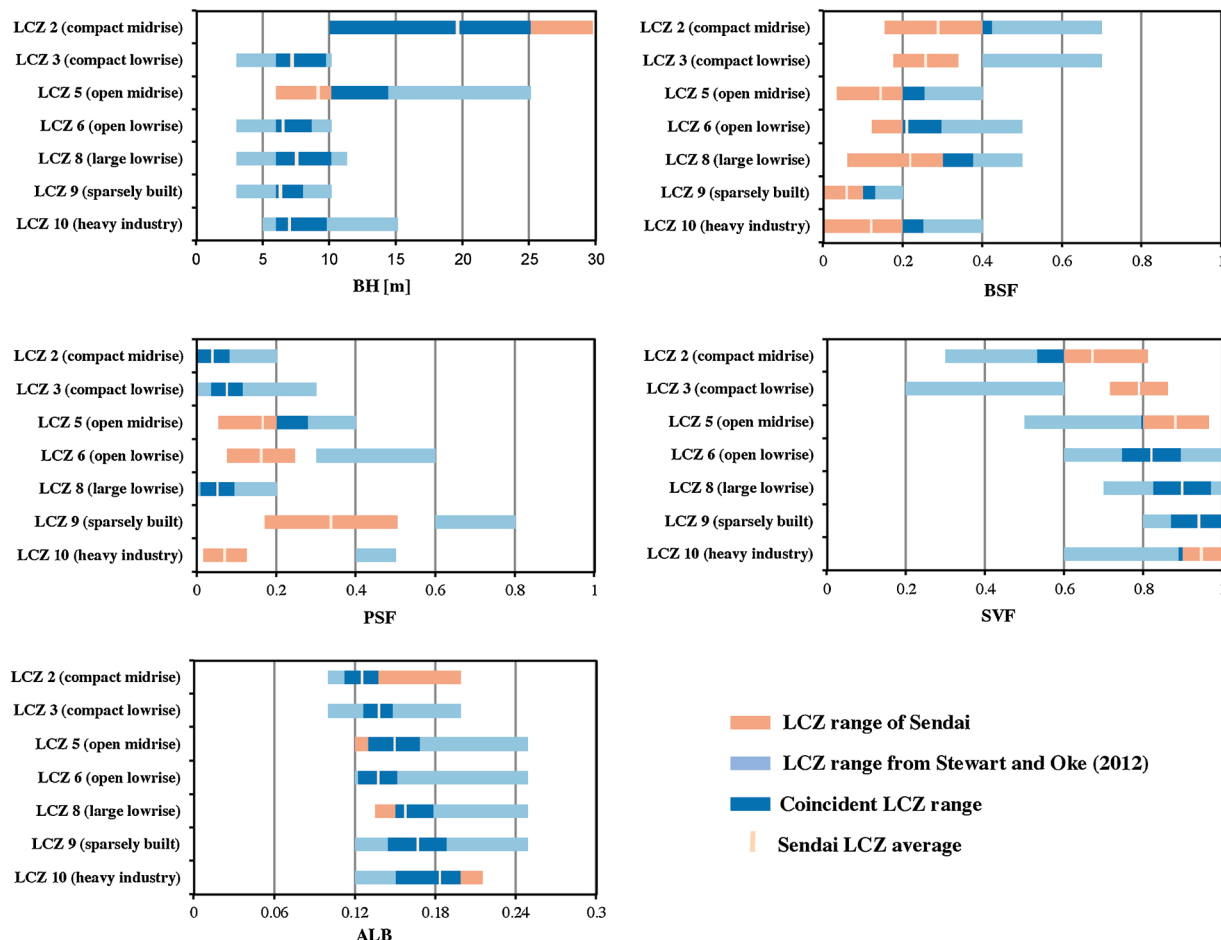


**Fig. 6.** LCZ parameter ranges determined for Sendai, compared to those recommended by [Stewart and Oke \(2012\)](#).

**Table 6**

Summary of LST in each LCZ in Sendai during the daytime and nighttime.

LCZ	Daytime (°C)				Nighttime (°C)			
	Max.	Min.	Mean	SD	Max.	Min	Mean	SD
LCZ 2 (compact mid-rise)	31.42	29.65	30.89	0.25	30.42	30.08	30.23	0.06
LCZ 3 (compact low-rise)	32.31	29.86	31.12	0.18	30.56	29.85	30.15	0.08
LCZ 5 (open mid-rise)	31.49	29.64	30.75	0.32	30.52	29.43	30.11	0.11
LCZ 6 (open low-rise)	31.72	29.90	30.97	0.24	31.35	29.66	30.06	0.09
LCZ 8 (large low-rise)	32.00	29.63	31.00	0.26	30.72	29.59	30.17	0.11
LCZ 9 (sparsely built)	31.96	29.49	30.51	0.27	30.55	29.63	29.99	0.12
LCZ 10 (heavy industry)	31.39	29.77	30.71	0.27	30.74	29.88	30.16	0.12
LCZ A (dense trees)	31.22	29.66	30.05	0.16	30.56	29.49	29.81	0.08
LCZ B (scattered trees)	31.38	29.68	30.39	0.25	30.50	29.66	29.92	0.11
LCZ D (low plants)	31.82	29.50	30.31	0.23	30.69	29.52	29.98	0.10
LCZ E (bare rock or paved)	31.64	30.47	31.10	0.20	30.51	30.14	30.34	0.10
LCZ F (bare soil or sand)	31.54	29.72	30.73	0.35	30.55	29.89	30.07	0.08

#### 4.3. Variation of LST in LCZs

Summary statistics of the daytime and nighttime LST in each LCZ, except for water bodies (LCZ G), are given in [Table 6](#). As the AST\_08 only includes surface temperatures for land areas ([NASA LP DAAC, 2001](#)), water bodies were not analyzed. While the mean LST values for all land area pixels were computed, the LST of each LCZ was averaged from the pixels of each LCZ type. The differences between the LST of each LCZ and the mean LST are shown in [Fig. 7](#).

Areas with dense trees (LCZ A) had the lowest LST during both the daytime and nighttime, while bare rock/paved areas (LCZ E) and compact low-rise areas (LCZ 3) had the highest LST during the nighttime and daytime, respectively. During the nighttime, LCZs with higher vegetation cover (PSF > 0.2), such as LCZ 9, D, B, and A, had low LSTs (LST < 29.99 °C); conversely, the LCZs with lower vegetation cover (PSF < 0.2), such as LCZ E, 2, and 8, had relatively high LSTs (LST > 30.17 °C).

Of the 10 LCZ built types, compact mid-rise areas (LCZ 2) had the lowest PSF and the highest LST during the nighttime, while sparsely built areas (LCZ 9) had the highest PSF and the lowest LST. Moreover, the built types LCZ 2, 3, 8, 10 in Sendai with lower PSFs were found to have higher LSTs during the nighttime compared with LCZ 5, 6, 9. During the daytime in Sendai, the mean LST of compact mid-rise areas (LCZ 2) was lower than that of compact low-rise areas (LCZ 3), and open mid-rise areas (LCZ 5) had a lower mean LST than open low-rise areas (LCZ 6).

To better understand the mechanism of the relationship between LCZs and SUHIs in Sendai, linear regression analyses were performed

between LST and LCZ properties of PSF, ALB, and SVF. These are shown in [Fig. 8](#). As the morphology information of urban areas is included in the SVF, the BH and BSF were not analyzed. In the nighttime, there was a strong negative correlation between nocturnal LST and PSF, with a coefficient of determination ( $R^2$ ) of 0.40. ALB and SVF had a very weak correlation with nocturnal LST, with  $R^2$  values of 0.034 and 0.045, respectively. In the daytime, both the PSF and SVF had a negative correlation with diurnal LST, with  $R^2$  values of 0.28 and 0.16.

#### 4.4. Variation of air temperature in LCZs

[Fig. 9a](#) and b show the mean diurnal and nocturnal air temperatures measured by the fixed loggers on Line P and Line Q, and the elevation of each logger. The northwestern loggers on the mountain side were positioned at higher elevations than the southeastern loggers on the coastal side of Sendai; in [Fig. 9a](#), logger CP indicates the division of the northwestern and southeastern groups. The mean thermal anomalies of each LCZ, relative to the mean air temperature measured by all loggers, are shown in [Fig. 9c](#).

During the nighttime, UHI effects are evident in both Lines P and Q and the air temperature measured by the loggers gradually increased as the logger positions drew closer to the urban center. The compact mid-rise areas (LCZ 2) had the highest nocturnal air temperature, while farmland (LCZ D) had the lowest; however, the nocturnal temperature of farmland on the mountain side, measured by logger EP, was higher than that measured by logger WP on the coastal side, even though both loggers were located in low plants areas (LCZ D) ([Fig. 9a, b](#)). Similarly, the nocturnal air temperature of compact low-rise areas (LCZ 3) and

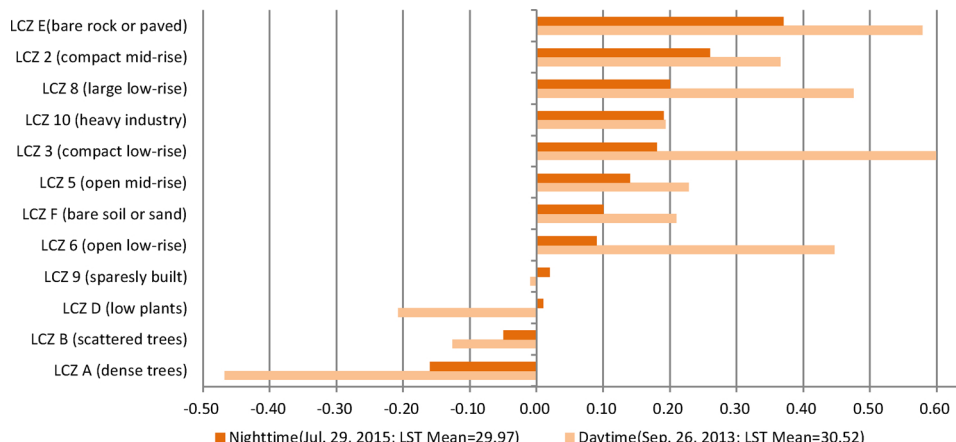


**Fig. 7.** Differences between the LST of each LCZ and the mean LST during the daytime and nighttime (unit: °C).

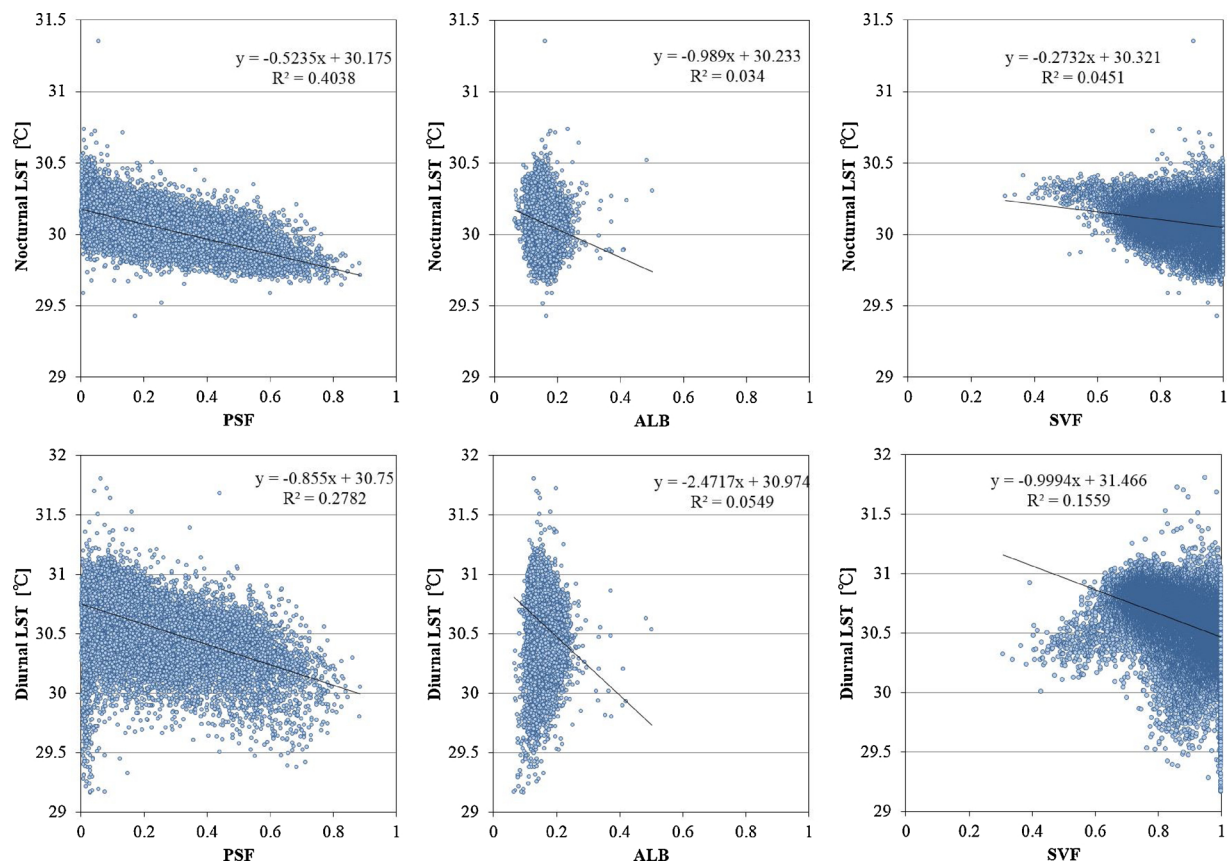


**Fig. 8.** Regression analysis between LST (y axis) and the LCZ properties (x axis) of PSF, ALB, and SVF in the daytime and nighttime.

open low-rise areas (LCZ 6) on the coastal side were higher than those on the mountain side. These differences are attributed to the cooling wind that blows from the mountains to the sea during the night. The air temperature of the open low-rise area on the mountain side (logger P2) was slightly cooler than the sparsely built area (logger P1) that was approximately 100 m lower in altitude. This difference may have been caused by the lapse rate, but it did not significantly affect the increasing trend of temperature from rural to urban areas. These results imply that the cooling effects of the nocturnal land breeze are significant in mountainside but weak in coastal urban areas.

The mean diurnal air temperatures in the metropolitan areas were generally higher than those in the rural areas for both Lines P and Q that exhibited the UHI phenomenon during the daytime. Nevertheless, the open low-rise area with 200-m elevation (logger P2) had the second lowest mean diurnal air temperature and its temperature was only slightly higher than that of the low plants area near the sea (Fig. 9a). Compared to the relatively cool air measured by logger P2 during the nighttime, the mean diurnal air temperature measured by logger P2 significantly influenced the increasing trend observed from rural to urban areas. Moreover, the sparsely built area located in the northern wind corridor (logger Q2) had a lower mean air temperature than the low plants area near the mountains (Fig. 9b). These results imply that the sea breeze can affect the LCZs in high elevations and those in the wind corridor without many obstacles, and can effectively reduce the diurnal air temperature.

## 5. Discussion

### 5.1. LCZ classification and properties of Japanese metropolitan areas

Based on the confusion matrix used to compare LCZ maps with training data, the WUDAPT L0 method has previously reported 96 %

overall accuracy (OA) for studies of both Houston, Texas and Kyiv, Ukraine (Bechtel et al., 2015; Danylo, See, Bechtel, Schepaschenko, & Fritz, 2016). However, the OA of the Kyiv study was only 64 %, when an independent dataset was used in place of the training data (Danylo et al., 2016). Studies of heterogeneous Chinese cities reported 64 % OA in Hong Kong (Ren et al., 2016), 76.31 % OA in Shanghai, and 75.5 % OA in Hangzhou (Cai et al., 2018), while higher OA has been reported for LCZ classifications of cities in Western Europe and North America, with homogenous urban morphologies. For example, the Belgian cities Ghent, Antwerp, and Brussels have reported 90.2 %, 85.7 %, and 79.6 % OA, respectively (Verdonck et al., 2017). Similarly, the OA of LCZ classifications of Phoenix and Las Vegas were 81.5 % and 81.9 %, respectively (Wang, Middel et al., 2018; Wang, Ren et al., 2018).

Our study also used a set of independent validation samples based on land use maps to assess the LCZ maps. The OA of the LCZ classification of Sendai was 92.59 %, which demonstrates that the WUDAPT L0 method is suitable for classifying Japanese cities. Nevertheless, since the WUDAPT L0 method is based on supervised machine learning methods, it requires local expert knowledge in order to select appropriate training samples (Wang, Middel et al., 2018; Wang, Ren et al., 2018). In the Human Influence Experiment (HUMINEX), LCZ maps developed by different operators using various TAs for a single city show obvious differences because of a lack of knowledge regarding recommendations for delineating TAs and because of an inadequate number of iterations (Bechtel et al., 2017). Furthermore, as the WUDAPT L0 method requires training samples to be greater than 1 km<sup>2</sup> to avoid getting a noisy output, misclassifications emerged from the discretization of a multidimensional space of morphologies (Bechtel et al., 2019) are inevitable. In the Asian cities like Nagpur, India and Colombo, Sri Lanka, plenty of LCZ sub-classes were detected, based on GIS and land use data (Kotharkar & Bagade, 2018; Perera & Emmanuel, 2018). These uncertain urban forms may confuse operators with

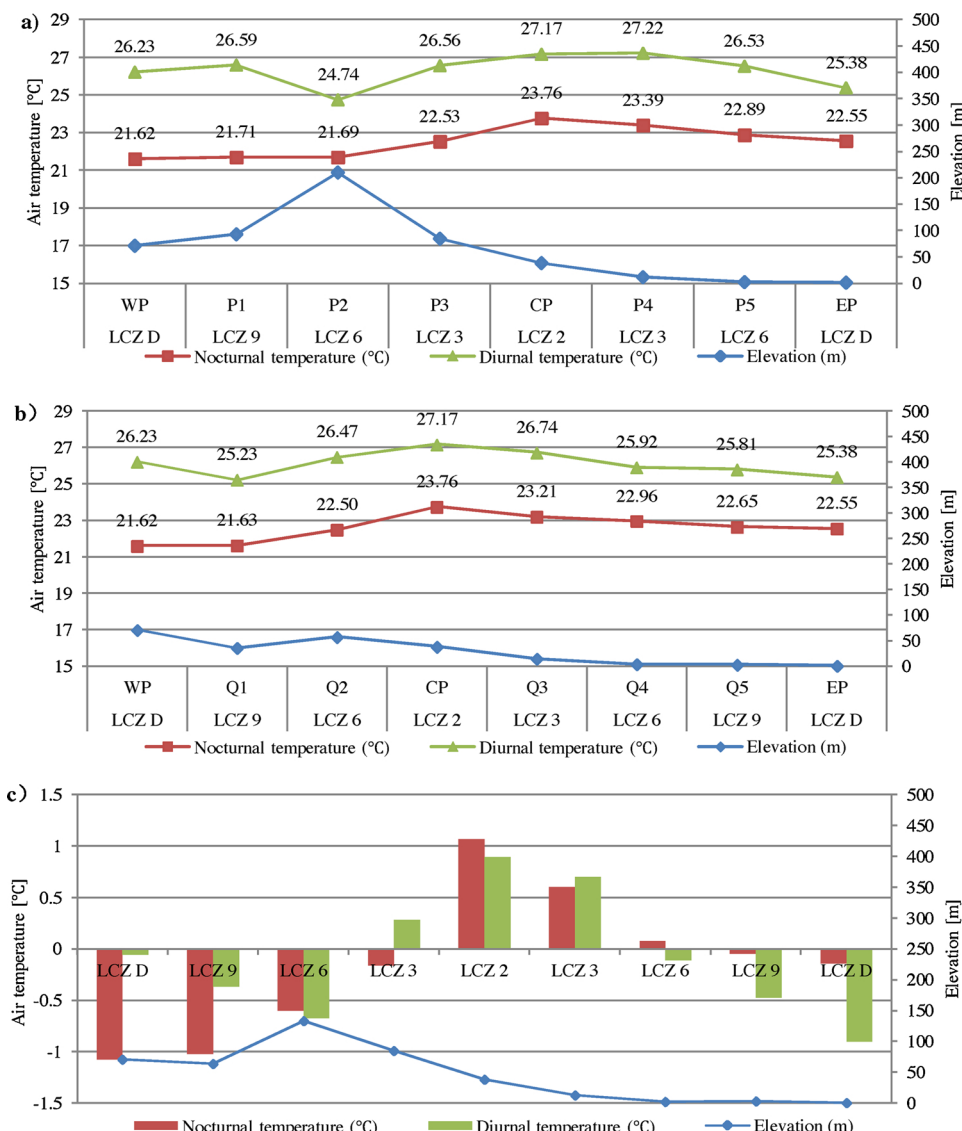


**Fig. 9.** Average air temperature and elevation of the fixed loggers on (a) Line P and (b) Line Q; (c) mean thermal anomalies relative to the mean air temperature measured by all loggers. The diurnal (6:00–18:30, JST) and nocturnal (21:00–5:00, JST) mean air temperatures were derived from data collected between August 11–22, 2018.

insufficient knowledge of the WUDAPT L0 method for selecting TAs, especially for heterogenous cities.

Through this case study of Sendai, we also found that it was difficult to classify urban areas using standard LCZ built types. For example, LCZ 2 was mixed with LCZ 2<sub>4</sub> and LCZ 4<sub>2</sub>. In order to avoid the confusion caused by this, we defined the linkages between standard LCZ built types and the sub-class LCZ built types (Fig. 1) before selecting TAs based on the roughly observed BH and BSF from Google Earth. Moreover, reference to an objective land use map helped the operators to do the adjustments in the iterative process of selecting TAs and conducting LCZ classification in Saga GIS. With these improvements of the WUDAPT L0 method, we obtained an LCZ map that was satisfactory.

In terms of the properties of LCZ built types, the BSFs and SVFs reported for Sendai were lower and higher than those reported by Stewart and Oke (2012), respectively. Divergence between the LCZ properties observed in specific local areas and those suggested by Stewart and Oke (2012) have also been reported by other studies

(Geletić & Lehnert, 2016; Leconte et al., 2015; Wang, Middel et al., 2018, Wang, Ren et al., 2018). Discrepancies in the BSFs and SVFs imply that the suggested properties may be suitable for selecting typical TAs, but not representative of mesoscale research. Geletić and Lehnert (2016) reported that accounting for specific regional features and the morphological character of built-up areas was essential to the success of the WUDAPT L0 method. Considering the unique characteristics of Japanese cities, the geometric and surface cover reference properties should be adjusted to accurately reflect the specific regional features. However, with respect to the universality and convenience of WUDAPT L0 in operation, we identified the sub-class LCZ built types according to the property ranges proposed by Stewart and Oke (2012) for each standard LCZ built type in Sendai. (Table 4)

## 5.2. Land surface temperature and air temperature

Although the LCZ scheme was originally designed to use air

temperature differences to quantify heat island magnitude (Stewart et al., 2014), we used it to determine the LST variation of each LCZ and consequently reduce the impact of unknown interference factors contributing to the UHI phenomenon. We found that both SVF and PSF have negative correlations with diurnal LST, while PSF significantly affected the nocturnal LST, demonstrated by linear regression analysis (Fig. 8). This exemplifies the importance of morphology and vegetation cover when classifying LCZs (Bechtel et al., 2015).

During the daytime, the LST of compact mid-rise (LCZ 2) was lower than the LST of compact low-rise (LCZ 3) and open low-rise (LCZ 6). Considering the PSFs of LCZ 3 and LCZ 6 were greater than LCZ 2, it implies that partial obstruction of the sun's rays by tall buildings reduced the LST (LCZ 2 had the lowest SVF). Conversely, the LST of built areas followed the expected trend during the nighttime: compact mid-rise (LCZ 2) > compact low-rise (LCZ 3) > open low-rise (LCZ 6) > sparsely built (LCZ 9). These results imply that the LCZ scheme can effectively connect land surface thermal information with urban built types which have various geometric and surface cover properties.

The LST during nighttime was consistent with the LCZ classification in Sendai; however, air temperature results did not match those from the LCZ scheme, because of sea-land breezes. In some cases, an LCZ built type had two different air temperatures; for example, the nocturnal air temperature of the open low-rise area on the coastal side of Sendai was warmer than the area on the mountain side because the nighttime wind coming down the mountain to the sea cooled the air in the western part of city. Therefore, the UHI magnitude ( $\Delta T_{Urban-Rural}$ ) of the mountain areas was higher than that of coastal areas at night (Fig. 9c). During the daytime, the cool sea breeze from the Pacific Ocean blows towards the mountain side and cools the air in the eastern part of city; thus, the coastal areas had higher UHI magnitudes during the day. Because the sea-land breeze travels in different directions during the day and night, the UHI magnitudes of the coastal areas in Sendai are different than those of the mountain areas. Therefore, the LCZ scheme must be used cautiously when analyzing UHI effects in regions exposed to sea-land breeze.

### 5.3. Comparison of UHI intensities in Sendai and other cities

Sea breeze and land breeze dominate the wind flow structure of coastal cities during the daytime and nighttime, respectively (Zhong & Takle, 1992), and the presence of mountains or slopes near the shore is expected to affect the sea-land breeze (Asai & Mitsumoto, 1978; Kitada, Igarashi, & Owada, 1986). Because Sendai has two types of urban-rural areas—the mountain side with high elevation and the coastal side with low elevation—the UHI magnitudes in the western and eastern areas of the city were different (Fig. 9c). As the cooling effect of the shallow land breeze was much stronger than the sea breeze in the nighttime

(Fig. 9), our results showed that the air temperature of the city center (LCZ 2) was not affected apparently by the sea orl and breezes. The nocturnal cooling air which decreased the air temperature in the urban areas on the mountain side, cannot reach the urban centers to cause significant influences on temperature of downtown areas on the coastal side.

In order to better understand the influence of land breeze on the nocturnal UHI phenomenon, UHI intensities of the entire study area in Sendai were compared to those of the basin city of Nagano, the mountain-coastal city of Matsuyama, and the plain-coastal cities of Dublin, Ireland and Vancouver, Canada (Table 7). Dublin and Vancouver are well-known metropolitan cities that are similar in size to Sendai, whereas Nagano and Matsuyama are small cities in Japan.

All of the Japanese cities have lower UHI intensities ( $\Delta T_{LCZ\ 2-D}$ ) than Dublin and Vancouver, which may be the result of lower BSFs and higher SVFs in Japanese cities, as well as regional climate. However, the  $\Delta T_{LCZ\ 2-D}$  values of the two small Japanese cities were greater than the mean value of Sendai, which is a metropolitan city. This phenomenon cannot be explained solely by geometric and land cover properties, but must also consider local winds. For example, the  $\Delta T_{LCZ\ 2-D}$  of mountain areas in Sendai was 2.1 K, which is slightly higher than that of Matsuyama (2 K), yet the  $\Delta T_{LCZ\ 2-D}$  of coastal areas in Sendai was only 1.2 K, which is less than that of Matsuyama. The land breeze that dominates the nighttime wind flow structure in these two mountain-coastal cities seems to cool the air in the rural areas on the mountain side more than the air in rural areas near the coast. Moreover, the wind cooling effect from the mountain side is more significant in Sendai, which has substantial elevation differences. In the basin city of Nagano, the cooling wind from the mountains reduces the air temperature in rural areas but not in urban centers, which contributes to the high UHI intensities in the urban centers.

While the  $\Delta T_{LCZ\ 2-3}$  of the mountain areas in Sendai were generally similar with those of both Nagano and Matsuyama, they were higher than those of Dublin with its plains. Conversely, the  $\Delta T_{LCZ\ 2-3}$  and  $\Delta T_{LCZ\ 2-6}$  of the coastal areas were more similar to those of Dublin. Although the  $\Delta T_{LCZ\ 2-6}$  of Dublin was 70 % higher than that of Sendai, the similarity between Dublin and the coastal side of Sendai is reasonable, considering that the open low-rise areas (LCZ 6) in Dublin have more vegetation cover. The UHI magnitude seems to follow a certain law that relates the influence of sea-land breeze to the LCZ classification; however, because the difference in air temperature over the land and ocean is the primary factor controlling the propulsion of local winds in coastal cities, the influence of sea surface temperature on sea-land-breeze, and subsequently UHIs, should be investigated in the future.

**Table 7**

Differences in the nighttime urban heat island intensities (LCZ x-LCZ y) of Sendai and other cities (Unit: K).

Urban-rural Comparison	Sendai			Nagano <sup>a</sup>	Matsuyama <sup>b</sup>	Dublin <sup>c</sup>	Vancouver <sup>d</sup>
	Mountain	Coast	Mean				
LCZ2-LCZD	2.1	1.2	1.7	3.2	2	4.2	6.3
LCZ3-LCZD	0.9	0.7	0.8	1.5	0.7	3.9	—
LCZ6-LCZD	0.5	0.2	0.3	1.2	0.5	2	4
Intra-urban Comparison							
LCZ2-LCZ3	1.2	0.5	0.8	1.7	1.3	0.5	—
LCZ2-LCZ6	1.7	1.0	1.3	2	1.5	2.2	2.3

<sup>a</sup> Mean temperature values of 90 evenings (22:00–02:00) measured by an automobile traveling across the basin (Stewart et al., 2014).

<sup>b</sup> Mean temperature values of 6 nights (21:00–06:00) measured by 3 fixed stations in Stevenson screens (Thapa Chhetri et al., 2017).

<sup>c</sup> Mean temperature value of 7 nights (21:00–06:00) measured by 6 fixed stations (Alexander & Mills, 2014).

<sup>d</sup> Temperature measured from an automobile traveling 3–5 h after sunset (2 h total) (Stewart et al., 2014).

#### 5.4. UHI mitigation strategies for Sendai

##### 5.4.1. Increasing vegetation cover in compact low-rise areas

We have found that the PSF have significantly negative correlations with nocturnal and diurnal LSTs. Moreover, the LST of compact low-rise areas (LCZ 3) was the highest during daytime. Since the sun's rays were partially obscured by tall buildings in compact mid-rise areas (LCZ 2), compact low-rise areas (LCZ 3) had the highest risk of heatstroke during the day in August. Consistent with our findings, the Fire and Disaster Management Agency reported that 46.6 % of emergency heatstroke victims in Japan between August 13th to 19th were found in their residences (including yards), which was substantially higher than the 14.3 % found in public areas outside of buildings (Fire & Disaster Management Agency, 2018).

Few plants are present along the streets and parking lots in the compact residential areas in Sendai, and there are only a few shrubs and low plants in the small yards of some dwellings. Therefore, we recommend that the vegetation cover in these areas is increased by planting more green plants along the streets and parking lots, and encouraging residents to plant trees with large canopies in their yards; this simple strategy could mitigate the risk of heatstroke in compact low-rise areas.

##### 5.4.2. Exploring and enhancing ventilation corridors to mitigate nocturnal UHIs

The mitigating effects of sea breeze and land breeze on UHI magnitude during the nighttime and daytime, respectively, were demonstrated by analyzing the differences in air temperature between LCZs. Because of the substantial differences in elevation in the urban areas of Sendai, a sea breeze that is taller than the height of a skyscraper (Fig. A2) can reach the inner urban areas of Sendai. Sea breeze can effectively cool the air in urban areas on the mountain side during the daytime; however, the cooling effects of the nocturnal land breeze were weakened by compact mid-rise areas because mountain winds are relatively shallow and near to the ground (Kagiya & Ashie, 2012). Our study determined that the nocturnal air temperatures of compact and open low-rise areas on the coastal side of Sendai are generally higher than those on the mountain side (Fig. 9). Therefore, naturally-existing ventilation corridors should be identified in order to allow the cooling wind from the mountains to reach the urban center and coastal areas; nocturnal UHIs could be mitigated by ventilation corridors along suitable roads and rivers that have low ground surface roughness and strong ventilation effects as a result of their wind field characteristics and land use plans. These ventilation corridors could then be enhanced by planting dense vegetation and controlling the height and density of buildings on both sides of the corridor (Kagiya & Ashie, 2013; Ren et al., 2018).

## 6. Conclusions

This study investigated the SUHI and UHI effects in Sendai, Japan using LCZ classifications derived from geometric and surface cover properties. We have demonstrated that the LCZ scheme can be used by urban planners to assess both SUHI and UHI effects and we have explained how the LCZ scheme can be used for cities that are exposed to sea-land breeze.

The three main results of this study are summarized below:

- 1) The WUDAPT L0 method was used to classify LCZ types in Sendai, a typical Japanese metropolitan city, and the OA of our LCZ classification was 92.59 %, using an independent dataset, which demonstrates that the WUDAPT L0 method is suitable for classifying Japanese cities. The GIS-derived geometric and surface cover properties also exhibited clear variations between the LCZ built types, even though the BSF and SVF in Sendai are very different than the ranges recommended by Stewart and Oke (2012). The geometric and surface cover properties used to classify LCZs must correspond to the specific regional features rather than simply using the recommended value.
- 2) The LST of each LCZ was determined in order to identify the factors contributing to the UHI phenomenon. During the nighttime, the LST was generally consistent with the LCZ classifications. Moreover, the LCZ scheme can also be used to analyze the surface thermal distribution during the daytime; for example, we found that the LST of compact residential areas was higher than that of the commercial areas in the city center.
- 3) Although the mitigating effects of sea breeze and land breeze affected different regional UHI magnitudes in Sendai, UHI assessments could be developed using the LCZ scheme. By dividing Sendai into western and eastern areas, with its compact urban center (LCZ 2) as the dividing line, the UHI magnitudes of the mountain side and coastal side can each be evaluated.

In some large coastal cities like Hong Kong and Tokyo, the city center is close to the coast and the rural areas are inland, which is very different from Sendai. Nevertheless, the UHI magnitudes may be different in different rural areas because of prevailing winds and/or local wind circulation systems. In this study we showed that by considering the different LCZ types and effects of sea-land breeze in different areas of a city, targeted analysis of UHI effects is feasible.

The LCZ scheme is a valuable innovation for urban climate research, as it allows for cross-city comparisons and also makes standard urban morphological data available. However, the geometric and surface cover properties used to classify LCZs should be adjusted to account for the geographical and meteorological features of the specific countries or regions being studied. Further evaluation of LCZ classification based on local thermal climates will highlight necessary changes to the LCZ scheme.

## Declaration of Competing Interest

The authors declare no conflicts of interest.

## Acknowledgements

This study was supported by the JSPS Grant-in-Aid for Scientific Research B No. 17H03349, JSPS KAKEN Challenging Research (Exploratory) No. 19K22004, the joint research project of the Wind Engineering Joint Usage/Research Center at Tokyo Polytechnic University No. 172010, and the China Scholarship Council No. 20160950013. This study was partially supported by the Vice-Chancellor's One-off Discretionary Fund of the Chinese University of Hong Kong.

## Appendix A

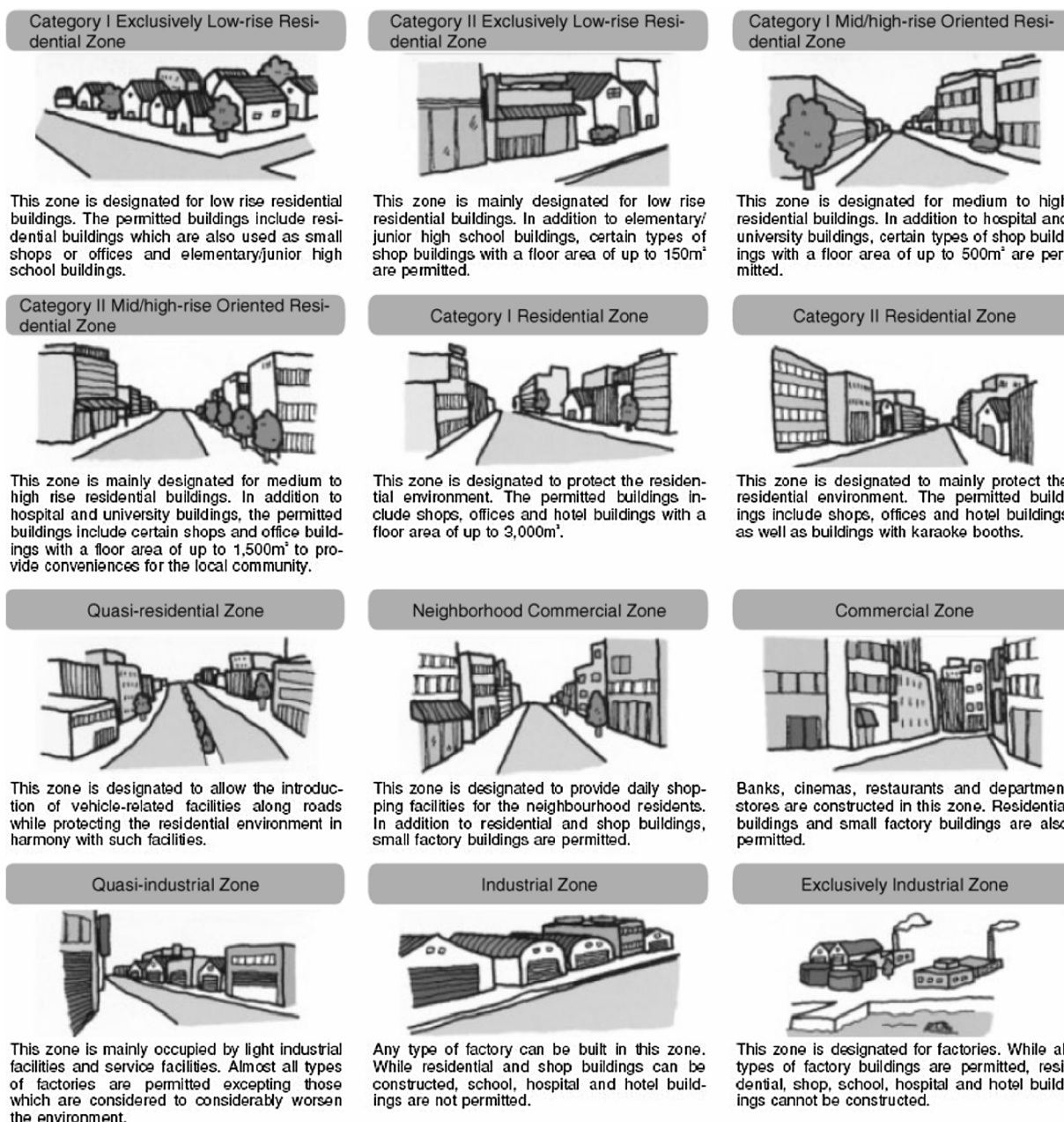


Fig. A1. Image of each land use zone's category (Japan International Cooperation Agency, 2007).

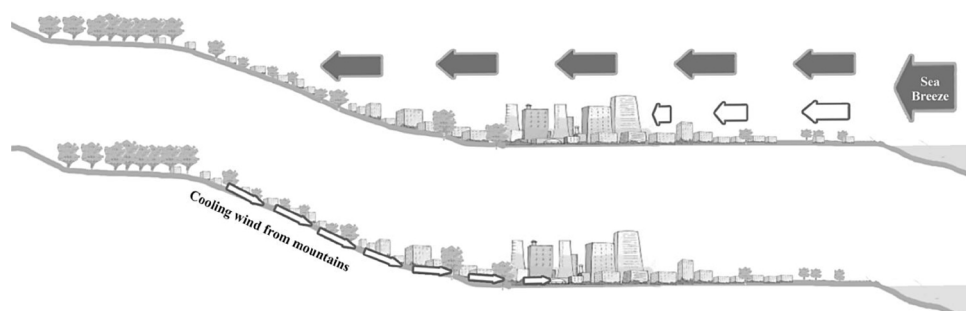


Fig. A2. Sea-land breeze during the daytime and nighttime in Sendai (revised from Kagiya & Ashie, 2012).

## References

- Alexander, P. J., & Mills, G. (2014). Local climate classification and Dublin's urban heat island. *Atmosphere*, 5(4), 755–774. <https://doi.org/10.3390/atmos5040755>.
- Alexander, P. J., Bechtel, B., Chow, W. T. L., Fealy, R., & Mills, G. (2016). Linking urban climate classification with an urban energy and water budget model: Multi-site and multi-seasonal evaluation. *Urban Climate*, 17, 196–215. <https://doi.org/10.1016/j.ulclim.2016.08.003>.
- Asai, T., & Mitsumoto, S. (1978). Effects of an inclined land surface on the land and sea breeze circulation: A numerical experiment. *Journal of the Meteorological Society of Japan*, 56, 559–570. <https://doi.org/10.2151/jmsj1965.56.6.559>.
- Bechtel, B., & Daneke, C. (2012). Classification of local climate zones based on multiple earth observation data. *IEEE Journal of Selected Topics in Applied Earth Observations and Remote Sensing*, 5(4), 1191–1202. <https://doi.org/10.1109/JSTARS.2012.2189873>.
- Bechtel, B., Alexander, P., Böhner, J., Ching, J., Conrad, O., Feddema, J., ... Stewart, I. (2015). Mapping local climate zones for a worldwide database of the form and function of cities. *ISPRS International Journal of Geo-information*, 4(1), 199–219. <https://doi.org/10.3390/ijgi4010199>.
- Bechtel, B., Demuzere, M., Sismanidis, P., Fenner, D., Brousse, O., Beck, C., ... Verdonck, M.-L. (2017). Quality of crowdsourced data on urban morphology—the human influence experiment (HUMINEX). *Urban Science*, 1, 15. <https://doi.org/10.3390/urbansci1020015>.
- Bechtel, B., Alexander, P. J., Beck, C., Böhner, J., Brousse, O., Ching, J., ... Xu, Y. (2019). Generating WUDAPT Level 0 data – Current status of production and evaluation. *Urban Climate*, 27, 24–45. <https://doi.org/10.1016/j.ulclim.2018.10.001>.
- Beck, C., Straub, A., Breitner, S., Cyrys, J., Philipp, A., Rathmann, J., ... Jacobbeit, J. (2018). Air temperature characteristics of local climate zones in the Augsburg urban area (Bavaria, southern Germany) under varying synoptic conditions. *Urban Climate*, 25, 152–166. <https://doi.org/10.1016/j.ulclim.2018.04.007>.
- Brousse, O., Martilli, A., Foley, M., Mills, G., & Bechtel, B. (2016). WUDAPT, an efficient land use producing data tool for mesoscale models? Integration of urban LCZ in WRF over Madrid. *Urban Climate*, 17, 116–134. <https://doi.org/10.1016/j.ulclim.2016.04.001>.
- Cai, M., Ren, C., Xu, Y., Lau, K. K. L., & Wang, R. (2018). Investigating the relationship between local climate zone and land surface temperature using an improved WUDAPT methodology – A case study of Yangtze River Delta, China. *Urban Climate*, 24, 485–502. <https://doi.org/10.1016/j.ulclim.2017.05.010>.
- Carlson, T. N., & Traci Arthur, S. (2000). The impact of land use - Land cover changes due to urbanization on surface microclimate and hydrology: A satellite perspective. *Global and Planetary Change*, 25(1–2), 49–65. [https://doi.org/10.1016/S0921-8181\(00\)00021-7](https://doi.org/10.1016/S0921-8181(00)00021-7).
- Conrad, O., Bechtel, B., Bock, M., Dietrich, H., Fischer, E., Gerlitz, L., ... Böhner, J. (2015). System for Automated Geoscientific Analyses (SAGA) v. 2.1.4. *Geoscientific Model Development*, 8(7), 1991–2007. <https://doi.org/10.5194/gmd-8-1991-2015>.
- Danylo, O., See, L., Bechtel, B., Schepaschenko, D., & Fritz, S. (2016). Contributing to WUDAPT: A local climate zone classification of two cities in Ukraine. *IEEE Journal of Selected Topics in Applied Earth Observations and Remote Sensing*, 9(5), 1841–1853. <https://doi.org/10.1109/JSTARS.2016.2539977>.
- Fenner, D., Meier, F., Scherer, D., & Polze, A. (2014). Spatial and temporal air temperature variability in Berlin, Germany, during the years 2001–2010. *Urban Climate*, 10(P2), 308–331. <https://doi.org/10.1016/j.ulclim.2014.02.004>.
- Fire and Disaster Management Agency (2018). 熱中症による救急搬送人員数: 8月13日～8月19日速報値 (the emergency conveyance number of people because of heat stroke: Aug. 13-Aug. 19 bulletin). [dataset] Available at: [https://www.fdma.go.jp/disaster/heatstroke/item/heatstroke003\\_sokuhouti07.pdf](https://www.fdma.go.jp/disaster/heatstroke/item/heatstroke003_sokuhouti07.pdf) (In Japanese).
- Gál, T., Bechtel, B., & Unger, J. (2015). Comparison of two different local climate zone mapping methods. *ICUC9-9th International Conference on Urban Climates*. July Available at [http://www.wudapt.org/wp-content/uploads/2015/07/Gal\\_etal\\_ICUC9.pdf](http://www.wudapt.org/wp-content/uploads/2015/07/Gal_etal_ICUC9.pdf).
- Geletić, J., & Lehnhert, M. (2016). GIS-based delineation of local climate zones: The case of medium-sized Central European cities. *Moravian Geographical Reports*, 24(3), 2–12. <https://doi.org/10.1515/mgr-2016-0012>.
- Geletić, J., Lehnhert, M., & Dobrovolný, P. (2016). Land surface temperature differences within local climate zones, based on two central European cities. *Remote Sensing*, 8(10), 1–18. <https://doi.org/10.3390/rs8100788>.
- Giridharan, R., & Emmanuel, R. (2018). The impact of urban compactness, comfort strategies and energy consumption on tropical urban heat island intensity: A review. *Sustainable Cities and Society*, 40, 677–687. <https://doi.org/10.1016/j.scs.2018.01.024>.
- Hiraishi, T., Yoneyama, N., Baba, Y., & Azuma, R. (2014). Field survey of the damage caused by the 2011 off the pacific coast of tohoku earthquake tsunami. In H. Kawase (Ed.). *Studies on the 2011 off the pacific coast of Tohoku earthquake* (pp. 37–48). Tokyo: Springer Japan. <https://doi.org/10.1007/978-4-431-54418-0>.
- Japan International Cooperation Agency (2007). *Urban land use planning system in Japan* (2nd edition). [https://jica-net-library.jica.go.jp/library/jn325/UrbanLandUsePlanningSystem\\_all.pdf](https://jica-net-library.jica.go.jp/library/jn325/UrbanLandUsePlanningSystem_all.pdf).
- Jones, G. W. (2017). Chapter 6: Urbanization trends in Asia: The conceptual and definitional challenges. In T. Champion, & G. Hugo (Eds.). *New forms of urbanization beyond the urban-rural dichotomy* (pp. 132–150). Farnham: Ashgate Publishing Ltd. <https://doi.org/10.1002/psp.340>.
- Junimura, J., & Watanabe, H. (2008). Study on the effects of sea breeze for decreasing urban air temperature in summer: Analyses based on long-term multi-point measurements and observed wind conditions. *Journal of Environmental Engineering AJ*, 73(623), 93–99. <https://doi.org/10.3130/ajie.73.93>.
- Kagiya, K., & Ashie, Y. (2012). National research project on Kaze-no-michi for city planning: Creation of ventilation paths of cool sea breeze in Tokyo. *Journal of Heat Island Institute International*, 7(2), 33–41. Available at: [http://ftp.heat-island.jp/web\\_journal/HII2009Conf/pdf/6.pdf](http://ftp.heat-island.jp/web_journal/HII2009Conf/pdf/6.pdf).
- Kagiya, K., & Ashie, Y. (2013). *Urban development guidance for urban heat island countermeasures utilizing "Kaze-no-michi"*. Available at: Japan: National Institute for Land and Infrastructure Management Ministry of Land, Infrastructure, Transport and Tourism. <http://www.nilim.go.jp/lab/bcg/siryou/tmn/tn0730pdf/ks0730.pdf>.
- Kaloustian, N., & Bechtel, B. (2016). Local climatic zoning and urban heat island in Beirut. *Procedia Engineering*, 169, 216–223. <https://doi.org/10.1016/j.proeng.2016.10.026>.
- Kaspersen, P. S., Fensholt, R., & Drews, M. (2015). Using Landsat vegetation indices to estimate impervious surface fractions for European cities. *Remote Sensing*, 7(6), 8224–8249. <https://doi.org/10.3390/rs70608224>.
- Kitada, T., Igarashi, K., & Owada, M. (1986). Numerical analysis of air pollution in a combined field of land/sea breeze and mountain/valley wind. *Journal of Applied Meteorology and Climatology*, 25, 767–784. [https://doi.org/10.1175-0450\(1986\)025<767:NAOAPI>2.0.CO;2](https://doi.org/10.1175-0450(1986)025<767:NAOAPI>2.0.CO;2).
- Kotharkar, R., & Bagade, A. (2018). Local climate zone classification for Indian cities: A case study of Nagpur. *Urban Climate*, 24, 369–392. <https://doi.org/10.1016/j.ulclim.2017.03.003>.
- Lau, K. K.-L., Chung, S. C., & Ren, C. (2019). Outdoor thermal comfort in different urban settings of sub-tropical high-density cities: An approach of adopting local climate zone (LCZ) classification. *Building and Environment*, 154, 227–238. <https://doi.org/10.1016/j.buildenv.2019.03.005>.
- Leconte, F., Bouyer, J., Claverie, R., & Pétrissans, M. (2015). Using Local Climate Zone scheme for UHI assessment: Evaluation of the method using mobile measurements. *Building and Environment*, 83, 39–49. <https://doi.org/10.1016/j.buildenv.2014.05.005>.
- Lelovics, E., Unger, J., Gál, T., & Gál, C. V. (2014). Design of an urban monitoring network based on Local Climate Zone mapping and temperature pattern modelling. *Climate Research*, 60(1), 51–62. <https://doi.org/10.3354/cr01220>.
- Li, S., & Jiang, G. M. (2018). Land surface temperature retrieval from Landsat-8 data with the generalized split-window algorithm. *IEEE Access*, 6, 18149–18162. <https://doi.org/10.1109/ACCESS.2018.2818741>.
- Liang, S. (2001). Narrowband to broadband conversions of land surface albedo I: Algorithms. *Remote Sensing of Environment*, 76(2), 213–238. [https://doi.org/10.1016/S0034-4257\(00\)00205-4](https://doi.org/10.1016/S0034-4257(00)00205-4).
- Middel, A., Brazel, A. J., Kaplan, S., & Myint, S. W. (2012). Daytime cooling efficiency and diurnal energy balance in Phoenix, Arizona, USA. *Climate Research*, 54(1), 21–34. <https://doi.org/10.3354/cr01103>.
- Myint, S. W., Wentz, E. A., Brazel, A. J., & Quattrochi, D. A. (2013). The impact of distinct anthropogenic and vegetation features on urban warming. *Landscape Ecology*, 28(5), 959–978. <https://doi.org/10.1007/s10980-013-9868-y>.
- NASA LP DAAC (2001). ASTER level 2 surface temperature product. NASA EOSDIS Land Processes DAAC [https://doi.org/10.5067/ASTER/AST\\_008.003](https://doi.org/10.5067/ASTER/AST_008.003) [dataset].
- Ng, E., Yuan, C., Chen, L., Ren, C., & Fung, J. C. H. (2011). Improving the wind environment in high-density cities by understanding urban morphology and surface roughness: A study in Hong Kong. *Landscape and Urban Planning*, 101(1), 59–74. <https://doi.org/10.1016/j.landurbplan.2011.01.004>.
- Parnell, S., & Walawege, R. (2011). Sub-Saharan African urbanisation and global environmental change. *Global Environmental Change Part A*, 21(SUPPL. 1), S12–S20. <https://doi.org/10.1016/j.gloenvcha.2011.09.014>.
- Peel, M. C., Finlayson, B. L., & McMahon, T. A. (2017). Updated world map of the Köppen-Geiger climate classification. *Hydrology and Earth System Sciences Discussions*, 11, 1633–1644. <https://doi.org/10.5194/hess-11-1633-2007>.
- Perera, N. G. R., & Emmanuel, R. (2018). Urban Climate A “Local Climate Zone” based approach to urban planning in Colombo. *Sri Lanka*, 23, 188–203. <https://doi.org/10.1016/j.ulclim.2016.11.006>.
- Population census of Japan (2015). Statistics bureau, ministry of internal affairs and communications of Japan. [dataset] <https://www.e-stat.go.jp/stat-search/files?page=1&layout=datatable&toukei=00200521&tstat=000001049104&cycle=0&tclass1=000001049105>.
- Ren, C., Wang, R., Cai, M., Xu, Y., Zheng, Y., & Ng, E. (2016). The accuracy of LCZ maps generated by the world Urban database and access Portal tools (WUDAPT) method: A case study of Hong Kong. *May Paper Read at 4th Int. Conf. Countermeasure Urban Heat Islands* <https://doi.org/10.1093/mnras/stv403>.
- Ren, C., Yang, R., Cheng, C., Xing, P., Fang, X., Zhang, S., ... Ng, E. (2018). Creating breathing cities by adopting urban ventilation assessment and wind corridor plan – The implementation in Chinese cities. *Journal of Wind Engineering and Industrial Aerodynamics*, 182, 170–188. <https://doi.org/10.1016/j.jweia.2018.09.023>.
- Salamanca, F., Martilli, A., Tewari, M., & Chen, F. (2011). A study of the urban boundary layer using different urban parameterizations and high-resolution urban canopy parameters with WRF. *Journal of Applied Meteorology and Climatology*, 50(5), 1107–1128. <https://doi.org/10.1175/2010JAMC2538.1>.
- Sasaki, K., Mochida, A., Yoshino, H., Watanabe, H., & Yoshida, T. (2008). A new method to select appropriate countermeasures against heat-island effects according to the regional characteristics of heat balance mechanism. *Journal of Wind Engineering and Industrial Aerodynamics*, 96(10–11), 1629–1639. <https://doi.org/10.1016/j.jweia.2008.02.035>.
- Shi, Y., Lau, K. K. L., Ren, C., & Ng, E. (2018). Evaluating the local climate zone classification in high-density heterogeneous urban environment using mobile

- measurement. *Urban Climate*, 25, 167–186. <https://doi.org/10.1016/j.ul clim.2018.07.001>.
- Stewart, I. D., & Oke, T. R. (2012). Local climate zone for urban temperature studies. *Bulletin of the American Meteorological Society*, 93(93), 1879–1900. <https://doi.org/10.1175/BAMS-D-11-00019.1>.
- Stewart, I. D., Oke, T. R., & Krayenhoff, E. S. (2014). Evaluation of the “local climate zone” scheme using temperature observations and model simulations. *International Journal of Climatology*, 34(4), 1062–1080. <https://doi.org/10.1002/joc.3746>.
- Thapa Chhetri, D. B., Fujimori, Y., & Moriaki, R. (2017). Local climate classification and urban heat/dry island in Matsuyama Plain. *Journal of Japan Society of Civil Engineers Ser B1*, 73(4), 487–492. [https://doi.org/10.2208/jcejhe.73.i\\_487](https://doi.org/10.2208/jcejhe.73.i_487).
- Tse, J. W. P., Yeung, P. S., Fung, J. C. H., Ren, C., Wang, R., Wong, M. M. F., ... CAI, M. (2018). Investigation of the meteorological effects of urbanization in recent decades: A case study of major cities in Pearl River Delta. *Urban Climate*, 26, 174–187. <https://doi.org/10.1016/j.ul clim.2018.08.007>.
- Urban Development Bureau of Sendai (2016). *Internet supportive service for the information of urban planning of Sendai*. [dataset] [http://www2.wagamachi-guide.com/sendai\\_tokei/map.asp](http://www2.wagamachi-guide.com/sendai_tokei/map.asp).
- Van de Voorde, T., Jacquet, W., & Canters, F. (2011). Mapping form and function in urban areas: An approach based on urban metrics and continuous impervious surface data. *Landscape and Urban Planning*, 102(3), 143–155. <https://doi.org/10.1016/j.landurbplan.2011.03.017>.
- Verdonck, M. L., Demuzere, M., Hooyberghs, H., Beck, C., Cyrys, J., Schneider, A., ... Van Coillie, F. (2018). The potential of local climate zones maps as a heat stress assessment tool, supported by simulated air temperature data. *Landscape and Urban Planning*, 178, 183–197. <https://doi.org/10.1016/j.landurbplan.2018.06.004>.
- Verdonck, M. L., Okujeni, A., van der Linden, S., Demuzere, M., De Wulf, R., & Van Coillie, F. (2017). Influence of neighbourhood information on ‘Local Climate Zone’ mapping in heterogeneous cities. *International Journal of Applied Earth Observation and Geoinformation*, 62, 102–113. <https://doi.org/10.1016/j.jag.2017.05.017>.
- Wan, Z. (2013). MODIS land surface temperature products users’ guide. Quality assurance (December), 33. Retrieved from [https://icess.eri.ucsb.edu/modis/LstUsrGuide/MODIS\\_LST\\_products\\_Users\\_guide\\_Collection-6.pdf](https://icess.eri.ucsb.edu/modis/LstUsrGuide/MODIS_LST_products_Users_guide_Collection-6.pdf).
- Wang, C., Middel, A., Myint, S. W., Kaplan, S., Brazel, A. J., & Lukasczyk, J. (2018). Assessing local climate zones in arid cities: The case of Phoenix, Arizona and Las Vegas, Nevada. *ISPRS Journal of Photogrammetry and Remote Sensing*, 141, 59–71. <https://doi.org/10.1016/j.isprsjprs.2018.04.009>.
- Wang, R., Ren, C., Xu, Y., Lau, K. K., & Shi, Y. (2018). Mapping the local climate zones of urban areas by GIS-based and WUDAPT methods: A case study of Hong Kong. *Urban Climate*, 24, 567–576. <https://doi.org/10.1016/j.ul clim.2017.10.001>.
- Weir, J., & Herring, D. (2000). *Measuring vegetation (NDVI&EVI)*. Available at: NASA Earth Observatory [https://earthobservatory.nasa.gov/features/MeasuringVegetation/measuring\\_vegetation\\_2.php](https://earthobservatory.nasa.gov/features/MeasuringVegetation/measuring_vegetation_2.php).
- Xu, Y., Ren, C., Cai, M., Edward, N. Y. Y., & Wu, T. (2017). Classification of local climate zones using ASTER and landsat data for high-density cities. *IEEE Journal of Selected Topics in Applied Earth Observations and Remote Sensing*, 10(7), 3397–3405. <https://doi.org/10.1109/JSTARS.2017.2683484>.
- Xu, Y., Ren, C., Ma, P., Ho, J., Wang, W., Lau, K. K. L., ... Ng, E. (2017). Urban morphology detection and computation for urban climate research. *Landscape and Urban Planning*, 167(February 2016), 212–224. <https://doi.org/10.1016/j.landurbplan.2017.06.018>.
- Yang, J., Jin, S., Xiao, X., Jin, C., Xia, J., Li, X., ... Wang, S. (2019). Local climate zone ventilation and urban land surface temperatures: Towards a performance-based and wind-sensitive planning proposal in megacities. *Sustainable Cities and Society*, 47, 101487. <https://doi.org/10.1016/j.scs.2019.101487>.
- Zheng, Y., Ren, C., Xu, Y., Wang, R., Ho, J., Lau, K., ... Ng, E. (2018). GIS-based mapping of local climate zone in the high-density city of Hong Kong. *Urban Climate*, 24, 419–448. <https://doi.org/10.1016/j.ul clim.2017.05.008>.
- Zhong, S., & Takle, E. S. (1992). An observational study of sea- and land-breeze circulation in an area of complex coastal heating. *Journal of Applied Meteorology*, 31, 1426–1438. [https://doi.org/10.1175/1520-0450\(1992\)031<1426:aososa>2.0.co;2](https://doi.org/10.1175/1520-0450(1992)031<1426:aososa>2.0.co;2).